



Article

A New Explicit Numerical Schemes for Time-Dependent PDEs with Application to Pressure Driven Fluid Flow in a Rectangular Duct

Yasir Nawaz ¹ , Muhammad Shoaib Arif ^{2,3,*} , Wasfi Shatanawi ^{2,4,5,*}  and Mairaj Bibi ⁶

¹ Department of Mathematics, Air University, PAF Complex E-9, Islamabad 44000, Pakistan; yasir_maths@yahoo.com

² Department of Mathematics and Sciences, College of Humanities and Sciences, Prince Sultan University, Riyadh 11586, Saudi Arabia

³ Stochastic Analysis and Optimization Research Group, Department of Mathematics, Air University, PAF Complex E-9, Islamabad 44000, Pakistan

⁴ Department of Mathematics, Faculty of Science, The Hashemite University, P.O. Box 330127, Zarqa 13133, Jordan

⁵ Department of Medical Research, China Medical University, Taichung 40402, Taiwan

⁶ Department of Mathematics, Comsats University Islamabad, Park Road Terlai Kalan, Islamabad 44000, Pakistan; mairaj_maths@comsats.edu.pk

* Correspondence: marif@psu.edu.sa (M.S.A.); wshatanawi@psu.edu.sa (W.S.)

Abstract: A modified class of temporal discretization schemes for partial differential equations (PDEs) is proposed, explicit and second to fifth-order accurate in time. In time, the stability region of the proposed modified second-order scheme is larger than the standard second-order Adams–Bashforth method constructed on two time levels. A modification made for the Du Fort–Frankel method was also implemented in the proposed second-order scheme, which permits the little larger stability region, but the scheme becomes first-order accurate. Since the Du Fort–Frankel method cannot be employed without a modification of averaging in time levels, the proposed second-order scheme can be used without any modification. The proposed modified scheme with different orders in space and second orders in time was implemented for heat and mass transfer of chemically reactive fluid flow in a rectangular duct. The flow is generated due to applying different pressure gradients. The contour plots of velocity, temperature, and concentration profiles are portrayed at different pressure gradients; Péclet number in heat transfer, Péclet number in mass transfer, reaction parameter, and at different times. In addition, stability and convergence conditions for the considered system of linear and non-linear PDEs consisting of non-dimensional momentum, energy, and concentration equations were found for two cases. The displayed graphs depict the transfer of heat in the fluid, which rises due to heated boundaries, and the transfer of mass in the fluid at various moments. Classical models can be solved using the proposed method, which has a faster convergence rate than the standard or classical approach. This approach is illustrated through computer simulations that demonstrate its key computational features. It is believed that the data presented in this study will serve as a useful source for future fluid flow investigations to be conducted in an industrial setting within an enclosed area.

Keywords: an explicit scheme; stability; fully developed fluid flow; heat and mass transfer; convergence



Citation: Nawaz, Y.; Arif, M.S.; Shatanawi, W.; Bibi, M. A New Explicit Numerical Schemes for Time-Dependent PDEs with Application to Pressure Driven Fluid Flow in a Rectangular Duct. *Energies* **2022**, *15*, 5145. <https://doi.org/10.3390/en15145145>

Academic Editor: Phillip Ligrani

Received: 15 June 2022

Accepted: 12 July 2022

Published: 15 July 2022

Publisher's Note: MDPI stays neutral with regard to jurisdictional claims in published maps and institutional affiliations.



Copyright: © 2022 by the authors. Licensee MDPI, Basel, Switzerland. This article is an open access article distributed under the terms and conditions of the Creative Commons Attribution (CC BY) license (<https://creativecommons.org/licenses/by/4.0/>).

1. Introduction

Applications of the magnetic field in MHD pump, heat exchangers, etc., has attracted many researchers' attention [1]. Hartmann (1998) formulated the electromagnetic viscous force [2]. However, unsteady MHD nanofluid compressed flow between parallel plates, observed by Dogonchi and Ganji [3,4], studied a similar effect with solar radiation. Ref. [5] recently analyzed unsteady magnetohydrodynamics (MHD) nanofluid flow using natural

conviction with entropy generation. Additionally, entropy formation in a non-Newtonian microflow regulated by conjugate heat transport was presented in [6].

Nayak and Redd et al. [7] studied the viscous dissipation effect and Maxwell liquid effect on MHD flow using thermal radiation. Refs. [8–10] depict some of the work on MHD flow through the variable surface topology.

The industrial applications of heat and mass transport using chemical reactions are substantial for many scientists. Route et al. [11] observed the chemical reaction, mass, and heat sources on MHD flow in an asymmetrical channel. Refs. [12,13] studied the effect of chemical reaction on convection flow of viscous nanofluid using a magnetic field and over a permeable sheet to solve the governing equation. In [14–16], fluid flows with effects of chemical reactions were studied using Jeffery liquid flow due to radially stretching sheets. Refs. [17–19] are some examples in which the chemical reaction effect was coupled with nanofluid, and resulting consequences were intimated on the industrial level. In [20], heat and mass transfer of upper-convected Maxwell nanofluid with the magnetic field's effects was studied past an inclined stretching surface. A shooting method consisting of the fourth-order Runge–Kutta method (RK4) was utilized to find the solution to ordinary differential equations (ODEs) obtained from PDEs.

One of the applications of Newtonian fluids is their use in lubrication. In lubrication, the fluid does not change viscosity as a function of shear, but it depends on the temperature. Motor oil is one example of this process. The oil does not become too thin at higher engine operating temperatures. Moreover, its important characteristic is that the viscosity does not change if this oil is shared between engine elements [21].

Various authors studied the flow in a duct for heat and mass transfer effects. The flow in a rectangular cross-section was given in [22], and the flow in a circular cross-section was given in [23,24]. The problem of flow in a rectangular duct with a constant streamwise pressure gradient was given in [25]. In [26], the authors focused on the entropy generation for viscoelastic fluid flow through a parallel plate microchannel under pressure gradient, interfacial slip, and conjugate heat transfer. The effect of viscous dissipation on convective heat transfer and entropy formation for Poiseuille flow in an asymmetrically heated slit microchannel was studied in [27].

An extensive literature study revealed that the amount of education based on blood flow in a porous saturated stenotic artery has dwindled. Dash et al. [28] studied blood flow in the tube via a homogenous porous medium. The central theme behind this study was that the distribution of fatty cholesterol and artery-clogging blood clots in the lumen of a coronary artery is equivalent to a fictitious porous medium in some pathological situations. This idea was manipulated by [29]. The blood was considered a Newtonian fluid and found its flow through a porous medium under magnetic field influence.

The present attempt proposes a new class of explicit numerical schemes for the temporal discretization of parabolic and first-order hyperbolic differential equations. These schemes are constructed at different time levels, and construction was made through the Taylor series expansions. A Von Neumann stability criterion was used to find the stability condition of the second-order scheme for a parabolic linear equation with diffusion term only. However, from a computation point of view, the scheme takes a small temporal step size to produce an accurate solution. In order to reduce the computational time, a modification is suggested. This suggested modification was used when the Du Fort–Frankel scheme was constructed from the second-order unconditionally unstable scheme. The modification in diffusion terms made the Du Fort–Frankel method unconditionally stable. A modification that made the Du Fort–Frankel method unconditionally stable is the average of two neighboring time levels to approximate the time at level “ n ”. Therefore, here, the same modification was implemented in the proposed scheme on the second-order central difference formula for diffusion term. Additionally, using this modification, the scheme permits a little larger time step size. Despite this, the scheme loses some of its temporal order as a result of this adjustment, and the application of a first-order approximation causes this loss of order. For obtaining second-order accuracy, one can use a third-order

approximation to approximate the time at level “n,” so the order of the modified scheme will not be affected if one can find the solution using the modified approach in an implicit manner. The work gave the third-order modification for the Du Fort–Frankel method [30]. Since the first-order approximation in the scheme permitted a little larger value of the diffusion number for the present flow problem, only the second-order proposed and the first-order modified scheme was used to produce the final results for the displayed graphs.

Since Adams–Bashforth’s methods are the class of methods used to solve the ordinary differential equations, in [30], a class of methods was given for temporal discretization of 1D hyperbolic partial differential equations. This class of methods [30] can give second to fifth-order accuracy for hyperbolic partial differential equations. In [31,32], a Fully Explicit and Compact Numerical Scheme of the Fourth Order for the Heat Transfer in Boundary Layer Flow was proposed and discussed.

The second-order Adams–Bashforth method for the temporal discretization of PDEs given in [28] can be employed for the following parabolic partial differential equation

$$\frac{\partial u}{\partial t} = \alpha \frac{\partial^2 u}{\partial x^2} \quad (1)$$

By using the existing numerical scheme, the discretized equation is given by

$$u_i^{n+1} = u_i^n + \frac{\alpha \Delta t}{2} \left\{ 3\delta_x^2 u_i^n - \delta_x^2 u_i^{n-1} \right\} \quad (2)$$

$$\text{where } \delta_x^2 u_i^n = \frac{u_{i-1}^n - 2u_i^n + u_{i+1}^n}{(\Delta x)^2}.$$

This method (2) is second-order accurate in space and time, which finds a solution at “n + 1” time level by using the previous two time levels, “n” and “n − 1”. This existing explicit method (2) has an advantage of accuracy over an existing Du Fort–Frankel method.

2. Proposed Numerical Scheme

This contribution is consisted on a similar kind of explicit class of schemes as given in Equation (2). For developing a scheme with a better stability region than existing scheme (2), the following modification is considered in the scheme given in Equation (2)

$$u_i^n \approx \frac{u_i^{n+1} + u_i^{n-1}}{2} \quad (3)$$

and so the proposed scheme for discretizing Equation (1) is given as

$$u_i^{n+1} = u_i^n + \frac{\alpha \Delta t}{2} \left\{ 3 \left(u_{i+1}^n - u_i^{n+1} - u_i^{n-1} + u_{i-1}^n \right) - \delta_x^2 u_i^{n-1} \right\} \quad (4)$$

In the initial stages of the this contribution, an explicit second-order numerical scheme of temporal discretization is proposed for time-dependent partial differential equations. Standard difference formulae or any other spatial discretization schemes can be used to discretize space variable(s). Additionally, stability and consistency for scalar equation and stability for the considered system of equations for heat and mass transfer of reactive chemical fluid flow in a rectangular duct are given.

The general difference form of discretized version of Equation (1) is given by

$$u_i^{n+1} = au_i^n + bu_i^{n-1} + \Delta t \left\{ c \left(\frac{\partial u}{\partial t} \right)_i^n + f \left(\frac{\partial u}{\partial t} \right)_i^{n-1} \right\} \quad (5)$$

The Taylor series expansions for u_i^{n+1} , u_i^{n-1} , and $\left(\frac{\partial u}{\partial t}\right)_i^{n-1}$ terms are given in Equation (3) as

$$u_i^{n+1} = u_i^n + \Delta t \left(\frac{\partial u}{\partial t}\right)_i^n + \frac{(\Delta t)^2}{2} \left(\frac{\partial^2 u}{\partial t^2}\right)_i^n + O((\Delta t)^3) \quad (6)$$

$$u_i^{n-1} = u_i^n - \Delta t \left(\frac{\partial u}{\partial t}\right)_i^n + \frac{(\Delta t)^2}{2} \left(\frac{\partial^2 u}{\partial t^2}\right)_i^n + O((\Delta t)^3) \quad (7)$$

$$\left(\frac{\partial u}{\partial t}\right)_i^{n-1} = \left(\frac{\partial u}{\partial t}\right)_i^n - \Delta t \left(\frac{\partial^2 u}{\partial t^2}\right)_i^n + O((\Delta t)^2) \quad (8)$$

Substituting (6)–(8) into Equation (5) gives

$$u_i^n + \Delta t \left(\frac{\partial u}{\partial t}\right)_i^n + \frac{(\Delta t)^2}{2} \left(\frac{\partial^2 u}{\partial t^2}\right)_i^n = au_i^n + bu_i^n - b\Delta t \left(\frac{\partial u}{\partial t}\right)_i^n + \frac{b(\Delta t)^2}{2} \left(\frac{\partial^2 u}{\partial t^2}\right)_i^n + \Delta t \left\{ c \left(\frac{\partial u}{\partial t}\right)_i^n + f \left(\frac{\partial u}{\partial t}\right)_i^n - f\Delta t \left(\frac{\partial^2 u}{\partial t^2}\right)_i^n \right\} \quad (9)$$

On equating the coefficients of u_i^n , $\Delta t \left(\frac{\partial u}{\partial t}\right)_i^n$ and $(\Delta t)^2 \left(\frac{\partial^2 u}{\partial t^2}\right)_i^n$ on both sides of Equation (9) gives

$$\left. \begin{aligned} a + b &= 1 \\ 1 &= -b + c + f \\ \frac{1}{2} &= \frac{b}{2} - f \end{aligned} \right\} \quad (10)$$

Solving Equation (10) gives

$$b = 1 - a, \quad c = \frac{4-a}{2}, \quad f = -\frac{a}{2} \quad (11)$$

Therefore, for second-order in time, an explicit scheme is given by

$$u_i^{n+1} = au_i^n + (1-a)u_i^{n-1} + \frac{\Delta t}{2} \left\{ (4-a) \left(\frac{\partial u}{\partial t}\right)_i^n - a \left(\frac{\partial u}{\partial t}\right)_i^{n-1} \right\} \quad (12)$$

Similarly, a scheme with temporal order of three can be constructed, which is given by

$$u_i^{n+1} = au_i^n + bu_i^{n-1} + cu_i^{n-2} + \Delta t \left\{ f \left(\frac{\partial u}{\partial t}\right)_i^n + g \left(\frac{\partial u}{\partial t}\right)_i^{n-1} + h \left(\frac{\partial u}{\partial t}\right)_i^{n-2} \right\} \quad (13)$$

where

$$c = 1 - a - b, \quad f = \frac{27 - 4a + b}{12}, \quad g = \frac{-4a - 2b}{3} \text{ and } h = \frac{9 - 4a - 5b}{12}$$

The mentioned scheme (13) consists of two free parameters, and schemes with orders four and five can be constructed similarly with three and four free parameters, respectively. Therefore, the class of Adams–Bashforth schemes for time-dependent PDEs is just a special case for the proposed schemes. Moreover, the second-order scheme with $a = 2$ gives the same stability region as produced by the second-order Runge–Kutta method, which is more than the standard second-order Adams–Bashforth method in PDEs.

For Equation (1), the scheme given in Equation (12) with $a = \frac{1}{2}$ can be expressed by

$$u_i^{n+1} = \frac{1}{2} (u_i^n + u_i^{n-1}) + \frac{\alpha \Delta t}{4(\Delta x)^2} \left\{ 7 \left(\frac{\partial^2 u}{\partial x^2}\right)_i^n - \left(\frac{\partial^2 u}{\partial x^2}\right)_i^{n-1} \right\} \quad (14)$$

If the second-order central difference formula for spatial discretization in Equation (14) is employed, then the resulting scheme is given as

$$u_i^{n+1} = \frac{1}{2} (u_i^n + u_i^{n-1}) + \frac{\alpha \Delta t}{4} \left\{ 7 \delta_x^2 u_i^n - \delta_x^2 u_i^{n-1} \right\} \quad (15)$$

In the next section, the stability of the numerical scheme is given using Von Neumann stability criteria for the following equation:

$$\frac{\partial u}{\partial t} = \alpha \left(\frac{\partial^2 u}{\partial y^2} + \frac{\partial^2 u}{\partial z^2} \right). \quad (16)$$

3. Scalar Stability

Discretize Equation (16) by using the constructed scheme in the previous section with second-order central spatial discretization. The discretize equation is given by

$$u_{i,j}^{n+1} = \frac{1}{2}(u_{i,j}^n + u_{i,j}^{n-1}) + \frac{\alpha \Delta t}{4(\Delta y)^2(\Delta z)^2} \left[\begin{aligned} & \{7(\Delta z)^2(u_{i+1,j}^n - 2u_{i,j}^n + u_{i-1,j}^n) + \\ & 7(\Delta y)^2(u_{i,j+1}^n - 2u_{i,j}^n + u_{i,j-1}^n) - \\ & (\Delta z)^2(u_{i+1,j}^{n-1} - 2u_{i,j}^{n-1} + u_{i-1,j}^{n-1}) - \\ & (\Delta y)^2(u_{i,j+1}^{n-1} - 2u_{i,j}^{n-1} + u_{i,j-1}^{n-1}) \} \end{aligned} \right] \quad (17)$$

In order to employ the Von Neumann stability criteria for Equation (17), consider the following transformations

$$\left. \begin{aligned} u_{i,j}^n &= \bar{U}^n e^{I(i\psi_1 + j\psi_2)}, & u_{i\pm 1,j}^n &= \bar{U}^n e^{I((i\pm 1)\psi_1 + j\psi_2)} \\ u_{i,j\pm 1}^n &= \bar{U}^n e^{I(i\psi_1 + (j\pm 1)\psi_2)}, & u_{i\pm 1,j}^{n-1} &= \bar{U}^{n-1} e^{I((i\pm 1)\psi_1 + j\psi_2)} \\ u_{i,j\pm 1}^{n-1} &= \bar{U}^{n-1} e^{I(i\psi_1 + (j\pm 1)\psi_2)}, & u_{i,j}^{n\pm 1} &= \bar{U}^{n\pm 1} e^{I(i\psi_1 + j\psi_2)} \end{aligned} \right\} \quad (18)$$

where $I = \sqrt{-1}$. Substituting transformations (18) into Equation (17) gives

$$\begin{aligned} \bar{U}^{n+1} e^{I(i\psi_1 + j\psi_2)} &= \frac{1}{2} (\bar{U}^n e^{I(i\psi_1 + j\psi_2)} + \bar{U}^{n-1} e^{I(i\psi_1 + j\psi_2)}) \\ &+ \frac{\alpha \Delta t}{4(\Delta y)^2(\Delta z)^2} \left[\begin{aligned} & 7\bar{U}^n \left\{ \begin{aligned} & (e^{I((i+1)\psi_1 + j\psi_2)} - 2e^{I(i\psi_1 + j\psi_2)} + e^{I((i-1)\psi_1 + j\psi_2)}) (\Delta z)^2 \\ & + (\Delta y)^2 (e^{I(i\psi_1 + (j+1)\psi_2)} - 2e^{I(i\psi_1 + j\psi_2)} + e^{I(i\psi_1 + (j-1)\psi_2)}) \end{aligned} \right\} \\ & - \bar{U}^{n-1} \left\{ \begin{aligned} & (\Delta z)^2 (e^{I((i+1)\psi_1 + j\psi_2)} - 2e^{I(i\psi_1 + j\psi_2)} + e^{I((i-1)\psi_1 + j\psi_2)}) \\ & + (\Delta y)^2 (e^{I(i\psi_1 + (j+1)\psi_2)} - 2e^{I(i\psi_1 + j\psi_2)} + e^{I(i\psi_1 + (j-1)\psi_2)}) \end{aligned} \right\} \end{aligned} \right] \end{aligned} \quad (19)$$

Dividing both sides of Equation (19) by $e^{I(i\psi_1 + j\psi_2)}$ gives

$$\bar{U}^{n+1} = \frac{1}{2}(\bar{U}^n + \bar{U}^{n-1}) + \frac{\alpha \Delta t}{4(\Delta y)^2(\Delta z)^2} \left[\begin{aligned} & 7\bar{U}^n \left\{ \begin{aligned} & (\Delta z)^2 (e^{I\psi_1} - 2 + e^{-I\psi_1}) \\ & + (\Delta y)^2 (e^{I\psi_2} - 2 + e^{-I\psi_2}) \end{aligned} \right\} \\ & - \bar{U}^{n-1} \left\{ \begin{aligned} & (\Delta z)^2 (e^{I\psi_1} - 2 + e^{-I\psi_1}) \\ & + (\Delta y)^2 (e^{I\psi_2} - 2 + e^{-I\psi_2}) \end{aligned} \right\} \end{aligned} \right] \quad (20)$$

Equation (20) can be expressed as

$$\bar{U}^{n+1} = \frac{1}{2}(\bar{U}^n + \bar{U}^{n-1}) + \frac{\alpha \Delta t}{2} \left[\begin{aligned} & 7\bar{U}^n \{ (\cos\psi_1 - 1)/(\Delta y)^2 + (\cos\psi_2 - 1)/(\Delta z)^2 \} \\ & - \bar{U}^{n-1} \{ (\cos\psi_1 - 1)/(\Delta y)^2 + (\cos\psi_2 - 1)/(\Delta z)^2 \} \end{aligned} \right] \quad (21)$$

Let $\bar{a} = \frac{1}{2} + \frac{7\alpha\Delta t}{2} [(\cos\psi_1 - 1)/(\Delta y)^2 + (\cos\psi_2 - 1)/(\Delta z)^2]$ and $\bar{b} = \frac{1}{2} - \frac{\alpha\Delta t}{2} [(\cos\psi_1 - 1)/(\Delta y)^2 + (\cos\psi_2 - 1)/(\Delta z)^2]$

Now, Equation (21) can be expressed as

$$\bar{U}^{n+1} = \bar{a}\bar{U}^n + \bar{b}\bar{U}^{n-1} \quad (22)$$

One more equation can be constructed as

$$\bar{U}^n = 1\bar{U}^n + 0\bar{U}^{n-1} \quad (23)$$

System of Equations (22) and (23) can be expressed in the following single matrix–vector of the form

$$\begin{bmatrix} \bar{U}^{n+1} \\ \bar{U}^n \end{bmatrix} = \begin{bmatrix} \bar{a} & \bar{b} \\ 1 & 0 \end{bmatrix} \begin{bmatrix} \bar{U}^n \\ \bar{U}^{n-1} \end{bmatrix} \quad (24)$$

The stability conditions can be imposed on the eigenvalues of the matrix given in (24) as

$$|\lambda_1| \leq 1 \text{ and } |\lambda_2| \leq 1 \quad (25)$$

where

$$\lambda_1 = \frac{\bar{a}}{2} - \frac{1}{2}\sqrt{\bar{a}^2 + 4\bar{b}} \text{ and } \lambda_2 = \frac{\bar{a}}{2} + \frac{1}{2}\sqrt{\bar{a}^2 + 4\bar{b}}$$

The most restrictive condition can be made by checking the expression $\bar{a}^2 + 4\bar{b}$ to be positive or negative or zero. Here, two cases were considered for extreme values of $\cos\psi_1$ and $\cos\psi_2$. For the first case, when $\cos\psi_1 = -1 = \cos\psi_2$, then the expression is $\bar{a}^2 + 4\bar{b}$ given by

$$\bar{a}^2 + 4\bar{b} = 49d^2 - 3d + \frac{9}{4} \quad (26)$$

Since the coefficient of d^2 is positive, its graph, which is a parabola, opens upwards, and by using optimization, it can also be proved that the vertex of the parabola (26) lies above to x -axis; due to these two mentioned facts, the expression (26) gives a positive value for every value of the diffusion number d for the considered case. For the second case, when $\cos\psi_1 = 1 = \cos\psi_2$, the expression $\bar{a}^2 + 4\bar{b}$ becomes zero, and the remaining two cases can be discussed similarly to the first case. Thus the eigenvalues are real, and the stability conditions can be found in inequalities $|\lambda_1| \leq 1$ and $|\lambda_2| \leq 1$. It is to be noted that the main contribution to stability condition can be found from two inequalities, $-2 \leq \bar{a} - \sqrt{\bar{a}^2 + 4\bar{b}}$ and $\bar{a} + \sqrt{\bar{a}^2 + 4\bar{b}} \leq 2$, and these inequalities can be implied from the inequalities $|\lambda_1| \leq 1$ and $|\lambda_2| \leq 1$.

Now, by using the inequality $-2 \leq \bar{a} - \sqrt{\bar{a}^2 + 4\bar{b}}$. The following inequality can be constructed: $\bar{b} \leq 1 + \bar{a}$, which gives

$$\frac{1}{2} + \alpha\Delta t \left(\frac{1}{(\Delta y)^2} + \frac{1}{(\Delta z)^2} \right) \leq 1 + \frac{1}{2} - 7\alpha\Delta t \left(\frac{1}{(\Delta y)^2} + \frac{1}{(\Delta z)^2} \right) \quad (27)$$

$$d \leq \frac{1}{8}$$

where $d = \alpha\Delta t \left(\frac{1}{(\Delta y)^2} + \frac{1}{(\Delta z)^2} \right)$.

Similarly, other two cases, when $\cos\psi_1 = -1$ and $\cos\psi_2 = 1$ or $\cos\psi_1 = 1$ and $\cos\psi_2 = -1$, can be discussed. The case when $\cos\psi_1 = 1$ and $\cos\psi_2 = 1$ is straightforward, and the inequality $\bar{b} \leq 1 + \bar{a}$ becomes true for every value of the diffusion number d . The remaining inequality to be checked is $\bar{a} + \sqrt{\bar{a}^2 + 4\bar{b}} \leq 2$, and from this inequality, one of the conditions that can be imposed on stability is that $2 - \bar{a} \geq 0$, which holds because $\max(\bar{a}) = \frac{1}{2}$ for $\alpha > 0$. Moreover, the inequality $\bar{a} + \sqrt{\bar{a}^2 + 4\bar{b}} \leq 2$ implies

$$1 - \bar{a} \leq \bar{b} \quad (28)$$

which gives $-7 \leq 1$ or $0 \leq 0$ for four different cases depending upon the extreme values of $\cos\psi_1$ and $\cos\psi_2$, and these inequalities are true for any choice of diffusion number d . The main contributing cases for stability were discussed, and the stability condition for the considered PDE is $d \leq \frac{1}{8}$.

4. Consistency of the Scheme

The consistency of the scheme is checked by employing Taylor series expansions for the terms in the scheme. Consider the scheme (17) for discretizing Equation (16) and the Taylor series expansions for the terms in Equation (17) are given as

$$u_{i+1,j}^n = u_{i,j}^n + \Delta y \left(\frac{\partial u}{\partial y} \right)_{i,j}^n + \frac{(\Delta y)^2}{2} \left(\frac{\partial^2 u}{\partial y^2} \right)_{i,j}^n + O((\Delta y)^3) \quad (29)$$

$$u_{i-1,j}^n = u_{i,j}^n - \Delta y \left(\frac{\partial u}{\partial y} \right)_{i,j}^n + \frac{(\Delta y)^2}{2} \left(\frac{\partial^2 u}{\partial y^2} \right)_{i,j}^n + O((\Delta y)^3) \quad (30)$$

Similarly, Taylor series expansions for the term $u_{i,j+1}^n$ and $u_{i,j-1}^n$ can be constructed. Now, some of the terms in the scheme (17) can be expressed by

$$7(\Delta z)^2(u_{i+1,j}^n - 2u_{i,j}^n + u_{i-1,j}^n) = 7(\Delta z)^2(\Delta y)^2 \left(\frac{\partial^2 u}{\partial y^2} \right)_{i,j}^n \quad (31)$$

$$7(\Delta y)^2(u_{i,j+1}^n - 2u_{i,j}^n + u_{i,j-1}^n) = 7(\Delta y)^2(\Delta z)^2 \left(\frac{\partial^2 u}{\partial z^2} \right)_{i,j}^n \quad (32)$$

Adding Equations (31) and (32) gives

$$7(\Delta z)^2(u_{i+1,j}^n - 2u_{i,j}^n + u_{i-1,j}^n) + 7(\Delta y)^2(u_{i,j+1}^n - 2u_{i,j}^n + u_{i,j-1}^n) = 7(\Delta z)^2(\Delta y)^2 \left\{ \left(\frac{\partial^2 u}{\partial y^2} \right)_{i,j}^n + \left(\frac{\partial^2 u}{\partial z^2} \right)_{i,j}^n \right\} \quad (33)$$

Now, the Taylor series expansion for the terms $u_{i+1,j}^{n-1}$, $u_{i,j}^{n-1}$ and $u_{i-1,j}^{n-1}$ are given by

$$\begin{aligned} u_{i+1,j}^{n-1} = u_{i,j}^n - \Delta t & \left(\frac{\partial u}{\partial t} \right)_{i,j}^n + \frac{(\Delta t)^2}{2} \left(\frac{\partial^2 u}{\partial t^2} \right)_{i,j}^n - \frac{(\Delta t)^3}{6} \left(\frac{\partial^3 u}{\partial t^3} \right)_{i,j}^n + \Delta y \left(\frac{\partial u}{\partial y} \right)_{i,j}^n - \Delta t \Delta y \left(\frac{\partial^2 u}{\partial y \partial t} \right)_{i,j}^n \\ & + \frac{(\Delta t)^2(\Delta y)}{2} \left(\frac{\partial^3 u}{\partial y \partial t^2} \right)_{i,j}^n - \frac{(\Delta t)^3(\Delta y)}{6} \left(\frac{\partial^4 u}{\partial y \partial t^3} \right)_{i,j}^n + \frac{(\Delta y)^2}{2} \left(\frac{\partial^2 u}{\partial y^2} \right)_{i,j}^n - \frac{(\Delta t)(\Delta y)^2}{2} \left(\frac{\partial^3 u}{\partial y^2 \partial t} \right)_{i,j}^n \\ & + \frac{(\Delta t)^2(\Delta y)^2}{4} \left(\frac{\partial^4 u}{\partial y^2 \partial t^2} \right)_{i,j}^n - \frac{(\Delta t)^3(\Delta y)^2}{12} \left(\frac{\partial^5 u}{\partial y^2 \partial t^3} \right)_{i,j}^n + \frac{(\Delta y)^3}{6} \left(\frac{\partial^3 u}{\partial y^3} \right)_{i,j}^n - \frac{(\Delta t)(\Delta y)^3}{6} \left(\frac{\partial^4 u}{\partial y^3 \partial t} \right)_{i,j}^n \\ & + \frac{(\Delta t)^3(\Delta y)^3}{12} \left(\frac{\partial^5 u}{\partial y^3 \partial t^2} \right)_{i,j}^n - \frac{(\Delta t)^3(\Delta y)^3}{36} \left(\frac{\partial^6 u}{\partial y^3 \partial t^3} \right)_{i,j}^n + O((\Delta t)^4, (\Delta y)^3) \end{aligned} \quad (34)$$

$$u_{i-1,j}^{n-1} = u_{i,j}^n - \Delta t \left(\frac{\partial u}{\partial t} \right)_{i,j}^n + \frac{(\Delta t)^2}{2} \left(\frac{\partial^2 u}{\partial t^2} \right)_{i,j}^n - \frac{(\Delta t)^3}{6} \left(\frac{\partial^3 u}{\partial t^3} \right)_{i,j}^n + O((\Delta t)^4) \quad (35)$$

$$\begin{aligned} u_{i-1,j}^{n-1} = u_{i,j}^n - \Delta t & \left(\frac{\partial u}{\partial t} \right)_{i,j}^n + \frac{(\Delta t)^2}{2} \left(\frac{\partial^2 u}{\partial t^2} \right)_{i,j}^n - \frac{(\Delta t)^3}{6} \left(\frac{\partial^3 u}{\partial t^3} \right)_{i,j}^n - \Delta y \left(\frac{\partial u}{\partial y} \right)_{i,j}^n + \Delta t \Delta y \left(\frac{\partial^2 u}{\partial y \partial t} \right)_{i,j}^n \\ & - \frac{(\Delta t)^2(\Delta y)}{2} \left(\frac{\partial^3 u}{\partial y \partial t^2} \right)_{i,j}^n + \frac{(\Delta t)^3(\Delta y)}{6} \left(\frac{\partial^4 u}{\partial y \partial t^3} \right)_{i,j}^n + \frac{(\Delta y)^2}{2} \left(\frac{\partial^2 u}{\partial y^2} \right)_{i,j}^n - \frac{(\Delta t)(\Delta y)^2}{2} \left(\frac{\partial^3 u}{\partial y^2 \partial t} \right)_{i,j}^n \\ & + \frac{(\Delta t)^2(\Delta y)^2}{4} \left(\frac{\partial^4 u}{\partial y^2 \partial t^2} \right)_{i,j}^n - \frac{(\Delta t)^3(\Delta y)^2}{12} \left(\frac{\partial^5 u}{\partial y^2 \partial t^3} \right)_{i,j}^n - \frac{(\Delta y)^3}{6} \left(\frac{\partial^3 u}{\partial y^3} \right)_{i,j}^n + \frac{(\Delta t)(\Delta y)^3}{6} \left(\frac{\partial^4 u}{\partial y^3 \partial t} \right)_{i,j}^n \\ & - \frac{(\Delta t)^3(\Delta y)^3}{12} \left(\frac{\partial^5 u}{\partial y^3 \partial t^2} \right)_{i,j}^n + \frac{(\Delta t)^3(\Delta y)^3}{36} \left(\frac{\partial^6 u}{\partial y^3 \partial t^3} \right)_{i,j}^n + O((\Delta t)^4, (\Delta y)^3) \end{aligned} \quad (36)$$

Similarly, Taylor series expansion for the terms $u_{i,j+1}^{n-1}$ and $u_{i,j-1}^{n-1}$ can be constructed. By using (34)–(36), some terms in the scheme (17) for time level “ $n - 1$ ” can be simplified as

$$(\Delta z)^2(u_{i+1,j}^{n-1} - 2u_{i,j}^{n-1} + u_{i-1,j}^{n-1}) = (\Delta z)^2 \left\{ \begin{aligned} & (\Delta y)^2 \left(\frac{\partial^2 u}{\partial y^2} \right)_{i,j}^n - (\Delta t)(\Delta y)^2 \left(\frac{\partial^3 u}{\partial y^2 \partial t} \right)_{i,j}^n \\ & + \frac{(\Delta t)^2(\Delta y)^2}{2} \left(\frac{\partial^4 u}{\partial y^2 \partial t^2} \right)_{i,j}^n - \frac{(\Delta t)^3(\Delta y)^2}{6} \left(\frac{\partial^5 u}{\partial y^2 \partial t^3} \right)_{i,j}^n \end{aligned} \right\} \quad (37)$$

Similarly, using the Taylor series, the terms $u_{i,j-1}^{n-1}$ and $u_{i,j+1}^{n-1}$ can be expanded and simplified as

$$(\Delta y)^2(u_{i,j-1}^{n-1} - 2u_{i,j}^{n-1} + u_{i,j+1}^{n-1}) = (\Delta y)^2 \left\{ \begin{aligned} & (\Delta z)^2 \left(\frac{\partial^2 u}{\partial z^2} \right)_{i,j}^n - (\Delta t)(\Delta z)^2 \left(\frac{\partial^3 u}{\partial z^2 \partial t} \right)_{i,j}^n \\ & + \frac{(\Delta t)^2(\Delta z)^2}{2} \left(\frac{\partial^4 u}{\partial z^2 \partial t^2} \right)_{i,j}^n - \frac{(\Delta t)^3(\Delta z)^2}{6} \left(\frac{\partial^5 u}{\partial z^2 \partial t^3} \right)_{i,j}^n \end{aligned} \right\} \quad (38)$$

By adding Equations (37) and (38), the resulting equation is given as

$$\begin{aligned} & (\Delta z)^2(u_{i+1,j}^{n-1} - 2u_{i,j}^{n-1} + u_{i-1,j}^{n-1}) + (\Delta y)^2(u_{i,j-1}^{n-1} - 2u_{i,j}^{n-1} + u_{i,j+1}^{n-1}) \\ & = (\Delta y)^2(\Delta z)^2 \left\{ \left(\frac{\partial^2 u}{\partial y^2} \right)_{i,j}^n + \left(\frac{\partial^2 u}{\partial z^2} \right)_{i,j}^n \right\} - \Delta t(\Delta y)^2(\Delta z)^2 \left\{ \left(\frac{\partial^3 u}{\partial y^2 \partial t} \right)_{i,j}^n + \left(\frac{\partial^3 u}{\partial z^2 \partial t} \right)_{i,j}^n \right\} \\ & + \frac{(\Delta t)^2(\Delta y)^2(\Delta z)^2}{2} \left\{ \left(\frac{\partial^4 u}{\partial y^2 \partial t^2} \right)_{i,j}^n + \left(\frac{\partial^4 u}{\partial z^2 \partial t^2} \right)_{i,j}^n \right\} - \frac{(\Delta t)^3(\Delta y)^2(\Delta z)^2}{6} \end{aligned} \quad (39)$$

By using Equations (17), (33) and (39), and Taylor series expansions for the terms $u_{i,j}^{n+1}$ and $u_{i,j}^{n-1}$, the resulting equation is given by

$$\begin{aligned} u_{i,j}^n + \Delta t \left(\frac{\partial u}{\partial t} \right)_{i,j}^n &+ \frac{(\Delta t)^2}{2} \left(\frac{\partial^2 u}{\partial t^2} \right)_{i,j}^n + \frac{(\Delta t)^3}{6} \left(\frac{\partial^3 u}{\partial t^3} \right)_{i,j}^n \\ &= \frac{1}{2} \left\{ u_{i,j}^n + u_{i,j}^n - \Delta t \left(\frac{\partial u}{\partial t} \right)_{i,j}^n + \frac{(\Delta t)^2}{2} \left(\frac{\partial^2 u}{\partial t^2} \right)_{i,j}^n - \frac{(\Delta t)^3}{6} \left(\frac{\partial^3 u}{\partial t^3} \right)_{i,j}^n \right\} \\ &+ \frac{\alpha \Delta t}{4} \left[6 \left\{ \left(\frac{\partial^2 u}{\partial y^2} \right)_{i,j}^n + \left(\frac{\partial^2 u}{\partial z^2} \right)_{i,j}^n \right\} + \Delta t \left\{ \left(\frac{\partial^3 u}{\partial y^2 \partial t} \right)_{i,j}^n + \left(\frac{\partial^3 u}{\partial z^2 \partial t} \right)_{i,j}^n \right\} - \frac{(\Delta t)^2}{2} \left\{ \left(\frac{\partial^4 u}{\partial y^2 \partial t^2} \right)_{i,j}^n + \left(\frac{\partial^4 u}{\partial z^2 \partial t^2} \right)_{i,j}^n \right\} \right. \\ &\left. + \frac{(\Delta t)^3}{6} \left\{ \left(\frac{\partial^5 u}{\partial y^2 \partial t^3} \right)_{i,j}^n + \left(\frac{\partial^5 u}{\partial z^2 \partial t^3} \right)_{i,j}^n \right\} \right] \end{aligned} \quad (40)$$

Simplifying the terms in Equation (40) yields

$$\begin{aligned} \left(\frac{\partial u}{\partial t} \right)_{i,j}^n &= \alpha \left\{ \left(\frac{\partial^2 u}{\partial y^2} \right)_{i,j}^n + \left(\frac{\partial^2 u}{\partial z^2} \right)_{i,j}^n \right\} + \frac{\alpha \Delta t}{6} \left\{ \left(\frac{\partial^3 u}{\partial y^2 \partial t} \right)_{i,j}^n + \left(\frac{\partial^3 u}{\partial z^2 \partial t} \right)_{i,j}^n \right\} - \frac{\alpha (\Delta t)^2}{12} \left\{ \left(\frac{\partial^4 u}{\partial y^2 \partial t^2} \right)_{i,j}^n + \left(\frac{\partial^4 u}{\partial z^2 \partial t^2} \right)_{i,j}^n \right\} \\ &+ \frac{\alpha (\Delta t)^3}{36} \left\{ \left(\frac{\partial^5 u}{\partial y^2 \partial t^3} \right)_{i,j}^n + \left(\frac{\partial^5 u}{\partial z^2 \partial t^3} \right)_{i,j}^n \right\} - \frac{(\Delta t)}{6} \left(\frac{\partial^2 u}{\partial t^2} \right)_{i,j}^n - \frac{(\Delta t)^2}{6} \left(\frac{\partial^3 u}{\partial t^3} \right)_{i,j}^n \end{aligned} \quad (41)$$

By using the consistency criteria, and applying the limits $\Delta t \rightarrow 0$, $\Delta y \rightarrow 0$, $\Delta x \rightarrow 0$, the resulting equation becomes the original parabolic partial differential Equation (16) evaluated at the grid point (i, j) and at time level “ n ”. Thus the scheme is consistent. Now using Equation (16) in Equation (41), the leading error term in the scheme is given by $-\frac{3}{8}(\Delta t)^3 \left(\frac{\partial^3 u}{\partial t^3} \right)_{i,j}^n$.

5. Problem Formulation in Fluid Flow

Consider a fully developed laminar, incompressible flow in a rectangular duct with a streamwise constant pressure gradient. The cross-sectional area of a duct is shown in Figure 1. Let u be a velocity component along x -axis, T is the temperature of the fluid, and let C is the concentration poured into the fluid. Two boundaries of the duct are kept at a hot temperature T_w , and an ambient temperature is used for the left and right walls of the rectangular cross-sectional region. The flow is generated due to the constant pressure gradient exerted on the fluid. Dirichlet-type boundary conditions for velocity, temperature, and concentration are used for all four sides of a duct. The concentration is poured into the specified duct location from its bottom wall.

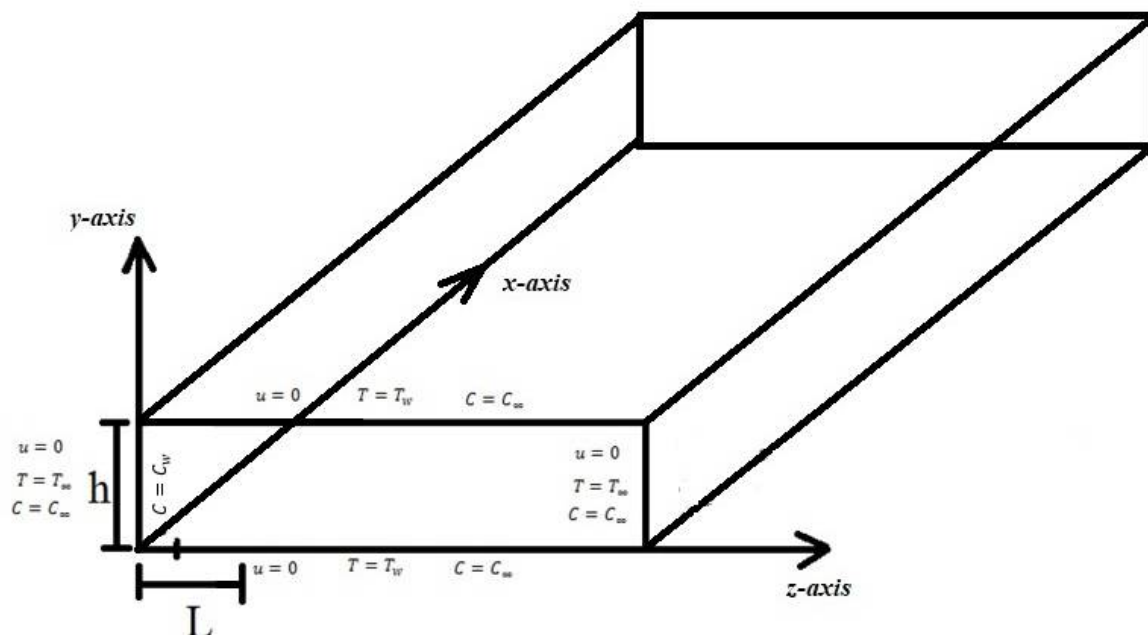


Figure 1. Two-dimensional geometry for the cross-section of rectangular duct.

The governing equations of the considered flow problem using the effect of the chemical reaction can be expressed as

$$\frac{\partial u}{\partial t} + \frac{1}{\rho} \frac{\partial p}{\partial x} = \nu \left(\frac{\partial^2 u}{\partial y^2} + \frac{\partial^2 u}{\partial z^2} \right) \quad (42)$$

$$\frac{\partial T}{\partial t} = \alpha \left(\frac{\partial^2 T}{\partial y^2} + \frac{\partial^2 T}{\partial z^2} \right) \quad (43)$$

$$\frac{\partial C}{\partial t} = D_B \left(\frac{\partial^2 C}{\partial y^2} + \frac{\partial^2 C}{\partial z^2} \right) - k_1 (C - C_\infty) \quad (44)$$

subject to the boundary conditions

$$\left. \begin{array}{l} \text{At } y = 0 \text{ and } y = h \\ (i) \quad 0 \leq z \leq 0.2360L \\ u = 0, T = T_h, C = C_1 \\ (ii) \quad z > 0.2360L \\ u = 0, T = T_h, C = C_0 \end{array} \right\} \quad (45)$$

$$\left. \begin{array}{l} \text{At } z = 0 \\ u = 0, T = T_c, C = C_0 \end{array} \right\} \quad (46)$$

$$\left. \begin{array}{l} \text{At } z = 7L \\ u = 0, T = 0, C = 0 \end{array} \right\} \quad (47)$$

where ρ is the density of the fluid, ν is the kinematic viscosity, α is the thermal diffusivity, D_B is the Brownian diffusion coefficient, and k_1 is the reaction rate parameter.

To make Equations (42)–(47) dimensionless, the following transformations are employed:

$$\left. \begin{array}{l} X = \frac{x}{L}, Y = \frac{y}{L}, Z = \frac{z}{L}, U = \frac{u}{u_0}, P = \frac{p}{\rho u_0^2} \\ \theta = \frac{T - T_\infty}{T_w - T_\infty}, \phi = \frac{C - C_\infty}{C_w - C_\infty}, \tau = \frac{t u_0}{L} \end{array} \right\} \quad (48)$$

where u_0 is the average velocity of the fluid. By incorporating transformations (48) for Equations (42)–(47), the following set of partial differential equations are obtained

$$\frac{\partial U}{\partial \tau} = -\frac{\partial P}{\partial X} + \frac{1}{Re} \left(\frac{\partial^2 U}{\partial Y^2} + \frac{\partial^2 U}{\partial Z^2} \right) \quad (49)$$

$$\frac{\partial \theta}{\partial \tau} = \frac{1}{Pe_1} \left(\frac{\partial^2 \theta}{\partial Y^2} + \frac{\partial^2 \theta}{\partial Z^2} \right) \quad (50)$$

$$\frac{\partial \phi}{\partial \tau} = \frac{1}{Pe_2} \left(\frac{\partial^2 \phi}{\partial Y^2} + \frac{\partial^2 \phi}{\partial Z^2} \right) - \gamma \phi \quad (51)$$

Subject to the dimensionless boundary conditions

$$\left. \begin{array}{l} \text{At } Y = 0 \text{ and } Y = \frac{h}{L} \\ (i) \quad 0 \leq Z \leq 0.2360 \\ U = 0, \theta = 1, \phi = 1 \\ (ii) \quad Z > 0.2360 \\ U = 0, \theta = 1, \phi = 0 \end{array} \right\} \quad (52)$$

$$\left. \begin{array}{l} \text{At } Z = 0 \\ U = 0, \theta = 0, \phi = 0 \end{array} \right\} \quad (53)$$

$$\left. \begin{array}{l} \text{At } Z = 7 \\ U = 0, \theta = 0, \phi = 0 \end{array} \right\} \quad (54)$$

where Re is the Reynolds number, Pe_1 and Pe_2 are the thermal and solutal Péclet numbers, respectively, and γ is the reaction rate parameter, which is defined by

$$Re = \frac{L u_0}{\nu}, Pe_1 = \frac{L u_0}{\alpha}, Pe_2 = \frac{L u_0}{D_B}, \gamma = \frac{k_1 L}{u_0} \quad (55)$$

To solve Equations (49)–(54), a proposed numerical scheme for temporal discretization is employed with second-order central differencing formulas are adopted for spatial discretization.

Using a proposed second-order scheme for temporal discretization with standard central difference formulas for the spatial discretization to Equations (49)–(51) yields the following equation

$$U_{i,j}^{n+1} = \frac{1}{2}(U_{i,j}^n + U_{i,j}^{n-1}) + \frac{\Delta t}{4} \left[-7 \frac{\partial P}{\partial X} + \frac{1}{R_e} \{7\delta_Y^2 U_{i,j}^n + 7\delta_Z^2 U_{i,j}^n\} + \frac{\partial P}{\partial X} - \frac{1}{R_e} \{\delta_Y^2 U_{i,j}^{n-1} + \delta_Z^2 U_{i,j}^{n-1}\} \right] \quad (56)$$

$$\theta_{i,j}^{n+1} = \frac{1}{2}(\theta_{i,j}^n + \theta_{i,j}^{n-1}) + \frac{\Delta t}{4} \left[\frac{1}{P_r} \{7\delta_Y^2 \theta_{i,j}^n + 7\delta_Z^2 \theta_{i,j}^n\} - \frac{1}{P_r} \{\delta_Y^2 \theta_{i,j}^{n-1} + \delta_Z^2 \theta_{i,j}^{n-1}\} \right] \quad (57)$$

$$\phi_{i,j}^{n+1} = \frac{1}{2}(\phi_{i,j}^n + \phi_{i,j}^{n-1}) + \frac{\Delta t}{4} \left[\frac{1}{S_c} \{7\delta_Y^2 \phi_{i,j}^n + 7\delta_Z^2 \phi_{i,j}^n\} - \frac{1}{S_c} \{\delta_Y^2 \phi_{i,j}^{n-1} + \delta_Z^2 \phi_{i,j}^{n-1}\} \right] \quad (58)$$

where $\delta_Y^2 U_{i,j}^n = \frac{U_{i-1,j}^n - 2U_{i,j}^n + U_{i+1,j}^n}{(\Delta Y)^2}$ and similarly, the remaining quantities in Equations (56) and (58) can be defined. The summary for finding solutions of Equations (49)–(54) using Matlab software is given in the form of Algorithm 1.

Algorithm 1 Summary of the Matlab code

1. Initialization	Begin The Code With Input Data.
2. Temporal For Loop	Begin The “For Loop” for Temporal Variable First and Give Initial Conditions.
3. Spatial For Loops	Begin “For Loops” ($i = 0$ to $\text{length}(y)$) and ($j = 0$ to $\text{length}(z)$) for Spatial Variables and Give Boundary Conditions Using if-else Statements.
4. Processing	Find the Solution for U , θ , and ϕ at the Grid Points (i, j) and at Time Level “ $n + 1$ ”.
5. End	End the Conditional Statements if-else and also end the Spatial and Temporal Loops.
6. Plots	Draw the Desire Plots Using Matlab Command Window.

6. Vector Stability

In order to check the stability conditions for Equations (49)–(51), a Von Neumann stability criteria is adopted again for this case. Therefore, for doing so, first, convert the Equations (49)–(51) into a single following matrix–vector equation

$$\frac{\partial \mathbf{U}}{\partial \tau} = \bar{C} \left(\frac{\partial^2 \mathbf{U}}{\partial Y^2} + \frac{\partial^2 \mathbf{U}}{\partial Z^2} \right) \quad (59)$$

$$\text{where } \bar{C} = \begin{bmatrix} \frac{1}{Re} & 0 & 0 \\ 0 & \frac{1}{Pr} & 0 \\ 0 & 0 & \frac{1}{Sc} \end{bmatrix} \text{ and } \mathbf{U} = [U, \theta, \phi]^T.$$

Employing the proposed numerical scheme for temporal discretization with the second-order central scheme for spatial discretization for Equation (59) gives:

$$\mathbf{U}_{i,j}^{n+1} = \frac{1}{2}(\mathbf{U}_{i,j}^n + \mathbf{U}_{i,j}^{n-1}) + \bar{C} \frac{\Delta \tau}{4} [7\{\delta_Y^2 \mathbf{U}_{i,j}^n + \delta_Z^2 \mathbf{U}_{i,j}^n\} - \{\delta_Y^2 \mathbf{U}_{i,j}^{n-1} + \delta_Z^2 \mathbf{U}_{i,j}^{n-1}\}] \quad (60)$$

$$\text{where } \delta_Y^2 \mathbf{U}_{i,j}^n = \frac{\mathbf{U}_{i+1,j}^n - 2\mathbf{U}_{i,j}^n + \mathbf{U}_{i-1,j}^n}{(\Delta Y)^2}.$$

By inserting the following transformations

$$\mathbf{U}_{i,j}^{n+1} = \mathbf{E}^{n+1} e^{I(i\psi_1 + j\psi_2)}, \quad \mathbf{U}_{i\pm 1,j}^n = \mathbf{E}^n e^{I((i+1)\psi_1 + j\psi_2)}, \quad \mathbf{U}_{i,j\pm 1}^n = \mathbf{E}^n e^{I(i\psi_1 + (j+1)\psi_2)}, \quad \mathbf{U}_{i,j}^n = \mathbf{E}^n e^{I(i\psi_1 + j\psi_2)}$$

into Equation (60), it gives the following equation after dividing both sides of the resulting equation by $e^{I(i\psi_1 + j\psi_2)}$

$$\mathbf{E}^{n+1} = \frac{1}{2}(\mathbf{E}^n + \mathbf{E}^{n-1}) + \frac{\Delta \tau \bar{C}}{4(\Delta Y)^2(\Delta Z)^2} \begin{bmatrix} 7(\Delta Z)^2 \mathbf{E}^n \{e^{I\psi_1} - 2 + e^{-I\psi_1}\} + \\ 7(\Delta Y)^2 \mathbf{E}^n \{e^{I\psi_2} - 2 + e^{-I\psi_2}\} - \\ (\Delta Z)^2 \mathbf{E}^{n-1} \{e^{I\psi_1} - 2 + e^{-I\psi_1}\} - (\Delta Y)^2 \mathbf{E}^{n-1} \{e^{I\psi_2} - 2 + e^{-I\psi_2}\} \end{bmatrix} \quad (61)$$

Equation (61) can be expressed as

$$E^{n+1} = \frac{1}{2}(E^n + E^{n-1}) + \frac{\Delta\tau\bar{C}}{2(\Delta Y)^2(\Delta Z)^2} \begin{bmatrix} 7E^n(\Delta Z)^2(\cos\psi_1 - 1) + \\ 7E^n(\Delta Y)^2(\cos\psi_1 - 1) - (\Delta Z)^2E^{n-1}(\cos\psi_1 - 1) - \\ (\Delta Y)^2E^{n-1}(\cos\psi_2 - 1) \end{bmatrix} \quad (62)$$

Let

$$\bar{A} = \frac{1}{2} - \frac{\Delta\tau\bar{C}}{2(\Delta Y)^2(\Delta Z)^2} [7(\Delta Z)^2(\cos\psi_1 - 1) + 7(\Delta Y)^2(\cos\psi_2 - 1)]$$

$$\bar{B} = \frac{1}{2} - \frac{\Delta\tau\bar{C}}{2(\Delta Y)^2(\Delta Z)^2} [(\Delta Z)^2(\cos\psi_1 - 1) + (\Delta Y)^2(\cos\psi_2 - 1)]$$

where \bar{A} and \bar{B} can be expressed by

$$\bar{A} = \frac{I.D}{2} + 7d\bar{e}\bar{C} \text{ and } \bar{B} = \frac{I.D}{2} - d\bar{e}\bar{C}$$

with $\bar{e} = (\Delta Z)^2(\cos\psi_1 - 1) + (\Delta Y)^2(\cos\psi_2 - 1)$, $d = \frac{\Delta\tau}{2(\Delta Y)^2(\Delta Z)^2}$, $I = \sqrt{-1}$ and $I.D$ is an identity matrix.

By substituting \bar{A} and \bar{B} into Equation (53), the resulting equation can be expressed by

$$E^{n+1} = \bar{A}E^n + \bar{B}E^{n-1} \quad (63)$$

Consider now an equation of the form

$$E^n = I.DE^n + OE^{n-1} \quad (64)$$

System of Equations (63) and (64) can be expressed in the form of a matrix–vector equation given as

$$\begin{bmatrix} E^{n+1} \\ E^n \end{bmatrix} = \begin{bmatrix} \bar{A} & \bar{B} \\ I.D & 0 \end{bmatrix} \begin{bmatrix} E^n \\ E^{n-1} \end{bmatrix} \quad (65)$$

The stability conditions can be imposed on the eigenvalues of the matrix given in Equation (65) as

$$|\lambda_1|^2 \leq 1 \text{ and } |\lambda_2|^2 \leq 1 \quad (66)$$

where $\lambda_1 = \frac{A_1}{2} - \frac{1}{2}\sqrt{A_1^2 + 4B_1}$ and $\lambda_2 = \frac{A_1}{2} + \frac{1}{2}\sqrt{A_1^2 + 4B_1}$ and $A_1 = \frac{1}{2} + 7\lambda_{m,\bar{C}}d\bar{e}$, $B_1 = \frac{1}{2} - \lambda_{m,\bar{C}}d\bar{e}$.

In the expressions of A_1 and B_1 , $\lambda_{m,\bar{C}}$ denotes the maximum eigenvalues of the matrix \bar{C} .

Theorem 1. A presently proposed scheme tends to converge for the dimensionless conservative form of considered PDEs if the error made by the scheme at the first time level is bounded and the following condition holds

$$8\|B\| \left(\frac{1}{(\Delta Y)^2} + \frac{1}{(\Delta Z)^2} \right) + \frac{\|C\|}{2} \rightarrow 0$$

where $f = U^2$, $B = \begin{bmatrix} 1/Re & 0 & 0 \\ 0 & 1/Pe_1 & 0 \\ 0 & 0 & 1/Pe_2 \end{bmatrix}$ and $C = \begin{bmatrix} 0 & 0 & 0 \\ 0 & 0 & 0 \\ 0 & 0 & -1 \end{bmatrix}$

Proof. Non-dimensional form of Equations (43)–(45) can be expressed in the following matrix–vector form

$$\frac{\partial U}{\partial \tau} = B \left(\frac{\partial^2 U}{\partial Y^2} + \frac{\partial^2 U}{\partial Z^2} \right) + CU \quad (67)$$

By discretizing Equation (67) using the proposed scheme with second-order central difference formulas, the following equation is obtained:

$$U_{i,j}^{n+1} = \frac{1}{2}(U_{i,j}^n + U_{i,j}^{n-1}) + \frac{B}{4} \{ 7(\delta_Y^2 U_{i,j}^n + \delta_Z^2 U_{i,j}^n) - (\delta_Y^2 U_{i,j}^{n-1} + \delta_Z^2 U_{i,j}^{n-1}) \} + \frac{C}{4} (7U_{i,j}^n - U_{i,j}^{n-1}) \quad (68)$$

Let the exact discretized scheme for discretizing Equation (67) be given as

$$\hat{U}_{i,j}^{n+1} = \frac{1}{2}(\hat{U}_{i,j}^n + \hat{U}_{i,j}^{n-1}) + \frac{B}{4} \{ 7(\delta_Y^2 \hat{U}_{i,j}^n + \delta_Z^2 \hat{U}_{i,j}^n) - (\delta_Y^2 \hat{U}_{i,j}^{n-1} + \delta_Z^2 \hat{U}_{i,j}^{n-1}) \} + \frac{C}{4} (7\hat{U}_{i,j}^n - \hat{U}_{i,j}^{n-1}) \quad (69)$$

By subtracting Equation (69) from Equation (68), denoting $e_{i,j}^n = u_{i,j}^n - \hat{u}_{i,j}^n$, $e_{i,j}^{n-1} = u_{i,j}^{n-1} - \hat{u}_{i,j}^{n-1}$, the resulting Equation is given by

$$e_{i,j}^{n+1} = \frac{1}{2}(e_{i,j}^n + e_{i,j}^{n-1}) + \left(\frac{B}{4}(\delta_Y^2 + \delta_Z^2) + \frac{C}{4}\right)(7e_{i,j}^n - e_{i,j}^{n-1}) \quad (70)$$

By applying norms on both sides of Equation (70), the following inequality is obtained:

$$\|e_{i,j}^{n+1}\| \leq \frac{1}{2}(\|e_{i,j}^n\| + \|e_{i,j}^{n-1}\|) + \left\| \left(\frac{B}{4}(\delta_Y^2 + \delta_Z^2) + \frac{C}{4}\right)(7e_{i,j}^n - e_{i,j}^{n-1}) \right\| \quad (71)$$

By using inequality $\|\delta_Z^2 e_{i,j}^n\| \leq \frac{\|e_{i,j+1}^n\| + 2\|e_{i,j}^n\| + \|e_{i,j-1}^n\|}{2(\Delta Z)^2}$ at time level “ n ” and applying $e^n = \max_{1 \leq i \leq Ny, 1 \leq j \leq Nz} \|e_{i,j}^n\|$, the resulting inequality can be expressed as

$$e^{n+1} \leq \frac{1}{2}(e^n + e^{n-1}) + \|B\| \left(\frac{1}{(\Delta Y)^2} + \frac{1}{(\Delta Z)^2} \right) (7e^n + e^{n-1}) + \frac{\|C\|}{4} (7e^n + e^{n-1}) \quad (72)$$

Now, if $e^{n-1} = \max\{e^n, e^{n-1}\}$, then the Inequality (72) can be simplified as

$$e^{n+1} \leq \left\{ 1 + 8\|B\| \left(\frac{1}{(\Delta Y)^2} + \frac{1}{(\Delta Z)^2} \right) + 2\|C\| \right\} e^{n-1} + G \left(O((\Delta \tau)^2, (\Delta Y)^2, (\Delta Z)^2) \right) \quad (73)$$

Let $\beta = 1 + 8\|B\| \left(\frac{1}{(\Delta Y)^2} + \frac{1}{(\Delta Z)^2} \right) + 2\|C\|$, then Inequality (73) can be expressed by

$$e^{n+1} \leq \beta e^{n-1} + G \left(O((\Delta \tau)^2, (\Delta Y)^2, (\Delta Z)^2) \right) \quad (74)$$

For $n = 1$ in Inequality (74), the following inequality is obtained

$$e^2 \leq \beta e^0 + G \left(O((\Delta \tau)^2, (\Delta Y)^2, (\Delta Z)^2) \right) \quad (75)$$

Since the initial condition is exact, so $e^0 = 0$; therefore, Inequality (75) becomes

$$e^2 \leq G \left(O((\Delta \tau)^2, (\Delta Y)^2, (\Delta Z)^2) \right) \quad (76)$$

By using the hypothesis, the following inequality can be constructed

$$e^1 \leq M \quad (77)$$

For $n = 2$ in Inequality (74), it gives

$$e^3 \leq \beta e^1 + G \left(O((\Delta \tau)^2, (\Delta Y)^2, (\Delta Z)^2) \right) \leq \beta M + G \left(O((\Delta \tau)^2, (\Delta Y)^2, (\Delta Z)^2) \right) \quad (78)$$

For $n = 3$ in Inequality (74), the following inequality is obtained

$$e^4 \leq \beta e^2 + G \left(O((\Delta \tau)^2, (\Delta Y)^2, (\Delta Z)^2) \right) \leq (1 + \beta) G \left(O((\Delta \tau)^2, (\Delta Y)^2, (\Delta Z)^2) \right) \quad (79)$$

For $n = 4$ in Inequality (74), it yields

$$e^5 \leq \beta e^3 + G \left(O((\Delta \tau)^2, (\Delta Y)^2, (\Delta Z)^2) \right) \leq \beta^2 M + (1 + \beta) G \left(O((\Delta \tau)^2, (\Delta Y)^2, (\Delta Z)^2) \right) \quad (80)$$

Similarly, this process continues, and for even n ,

$$e^n \leq (1 + \beta + \beta^2 + \dots + \beta^{n-2}) G \left(O((\Delta \tau)^2, (\Delta Y)^2, (\Delta Z)^2) \right) \quad (81)$$

When n is odd, an inequality becomes

$$e^n \leq \beta^{n-3} M + (1 + \beta + \beta^2 + \dots + \beta^{n-3}) G \left(O((\Delta \tau)^2, (\Delta Y)^2, (\Delta Z)^2) \right) \quad (82)$$

Since the series $1 + \beta + \beta^2 + \dots + \beta^{n-3} + \dots$ is a geometric series that converges for $|\beta| \leq 1$ and similarly if $e^n = \max\{e^n, e^{n-1}\}$, then it can be proved that $|\beta| \leq 1$ and therefore theorem is proved. \square

7. Results and Discussion

The set of governing non-dimensional partial differential equations was solved by employing the proposed second-order in time with second-order and combined second and fourth-order spatial discretization. The proposed second-order scheme was proved to be conditionally stable for the case of scalar parabolic partial differential equations. In addition to this, a modification was suggested that can be coupled with the proposed scheme, which permits a little larger stability region. However, it has the disadvantage of reduction in the order of accuracy. Since the modification is first-order accurate, the order of the resultant scheme is reduced, and the proposed scheme (4) and Du Fort–Frankel scheme become first-order accurate. However, since Richardson’s scheme was unconditionally unstable, the modification makes it unconditionally stable, and here, the same modification was used to enhance the stability region. The modification overcomes the computational time issue for a second-order scheme. Because a scheme with a very small temporal step size may take more time to converge compared to a scheme that may take a short time to converge, the disadvantage is dropping a temporal order of a scheme. However, one can use a third-order approximation instead of Du Fort–Frankel’s first-order approximation for the diffusion term. The third-order approximation [29], as mentioned in the introduction of this work, can also be considered, and so in this way, the order of the scheme is not reduced in some or most of the cases. Moreover, the Du Fort–Frankel method consists of the time derivative on “ n th” time level. For this case, the time derivatives were used for two consecutive time levels, “ n th” and “ $(n - 1)$ th”, but the modification is suggested for the “ n th” time level and with a spatial discretization of a diffusion term(s). The stability of the system of equations was also given.

In drawing Figures 2–12, $L = 1$ and $h = 1$ were used. Figure 1 shows the geometry of the cross-section of a rectangular duct. Dirichlet-type boundary conditions were implemented on all four sides of the rectangular cross-sectional region of the duct. The x coordinate is the streamwise coordinate of the flow, and the flow was generated due to different constant pressure gradients exerted on the fluid from the inlet. A small part of the bottom boundary was used for concentration. Therefore, in non-dimensional form, the concentration has a maximum value at the particular part of the boundary, and at the remaining boundaries, it is zero. Figure 2 shows the flow velocity at different pressure gradients. Since the fully developed flow was considered, the parabolic behavior of the velocity can be visualized in Figure 2.

Figure 3 shows velocity contours at different times. Since no-slip boundary conditions were imposed at the walls, the same color representing these conditions is shown in Figure 3.

Figure 3 shows that more layers of fluid are disturbing with time. Figure 4 shows the flow temperature with the variation in thermal Péclet number.

By decaying thermal Péclet number, the temperature of the flow de-escalates. This results from lower thermal conductivity due to a decrease in thermal diffusivity. The decay in thermal diffusivity is the consequence of the direct relationship between thermal diffusivity and thermal Péclet number. Figure 5 shows the contours of the temperature of the flow.

Since the temperature has its maximum values at the top and bottom edges of the rectangular region, the temperature of the fluid near these walls is maximum. Then, due to transferring heat into adjacent layers of the fluid, the temperature of those layers also increases. The increase in thermal Péclet number produces lower heat transfer, which can be seen in Figure 5. The decrease in the heat transfer by increment in thermal Péclet number is the consequence of decreasing thermal conductivity discussed earlier in this contribution. Figure 6 shows the contours of the temperature of the flow at different value times.

Figure 6 deliberates that more layers of fluid become hotter with time. The temperature has its minimum values at the left and right walls of the rectangular cross-sectional region. Figure 7 deliberates the temperature of the flow at different times and different z coordinates.

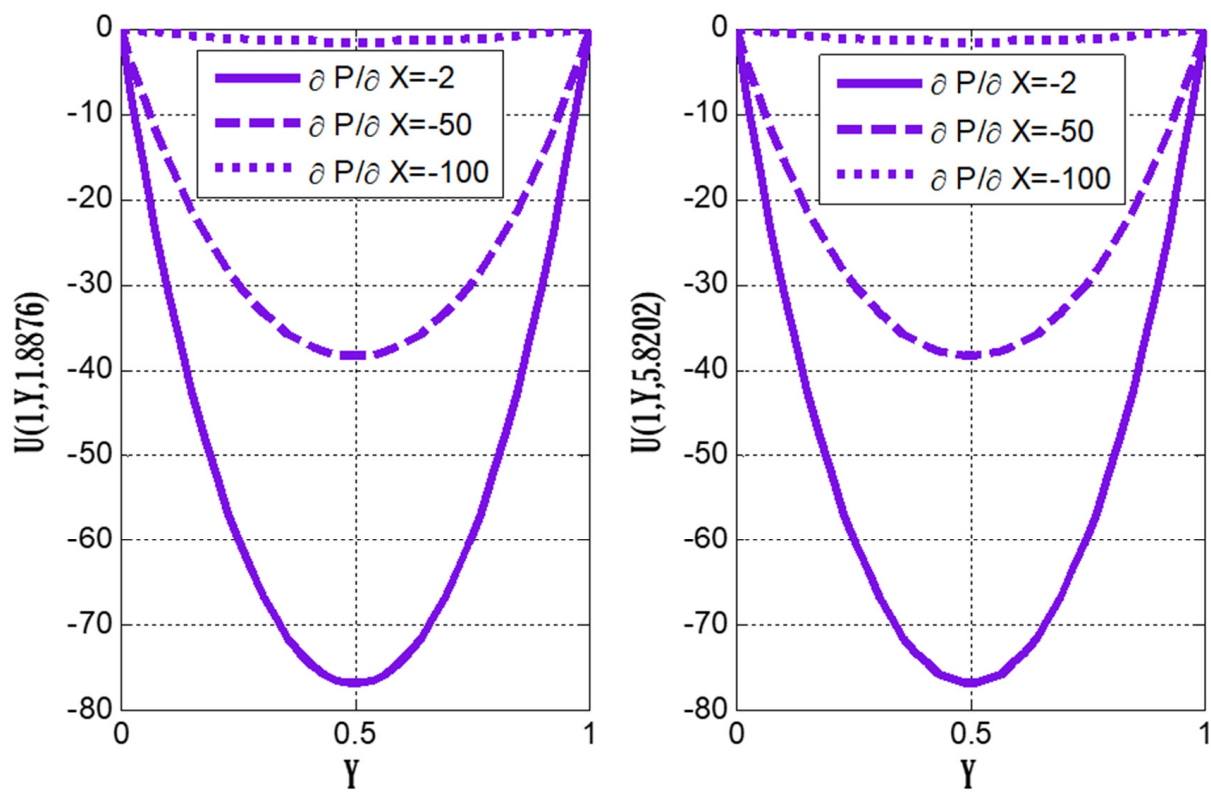


Figure 2. Impact of pressure gradient on velocity using $N_\tau = 3000$, $N_Y = 40$, $N_Z = 90$.

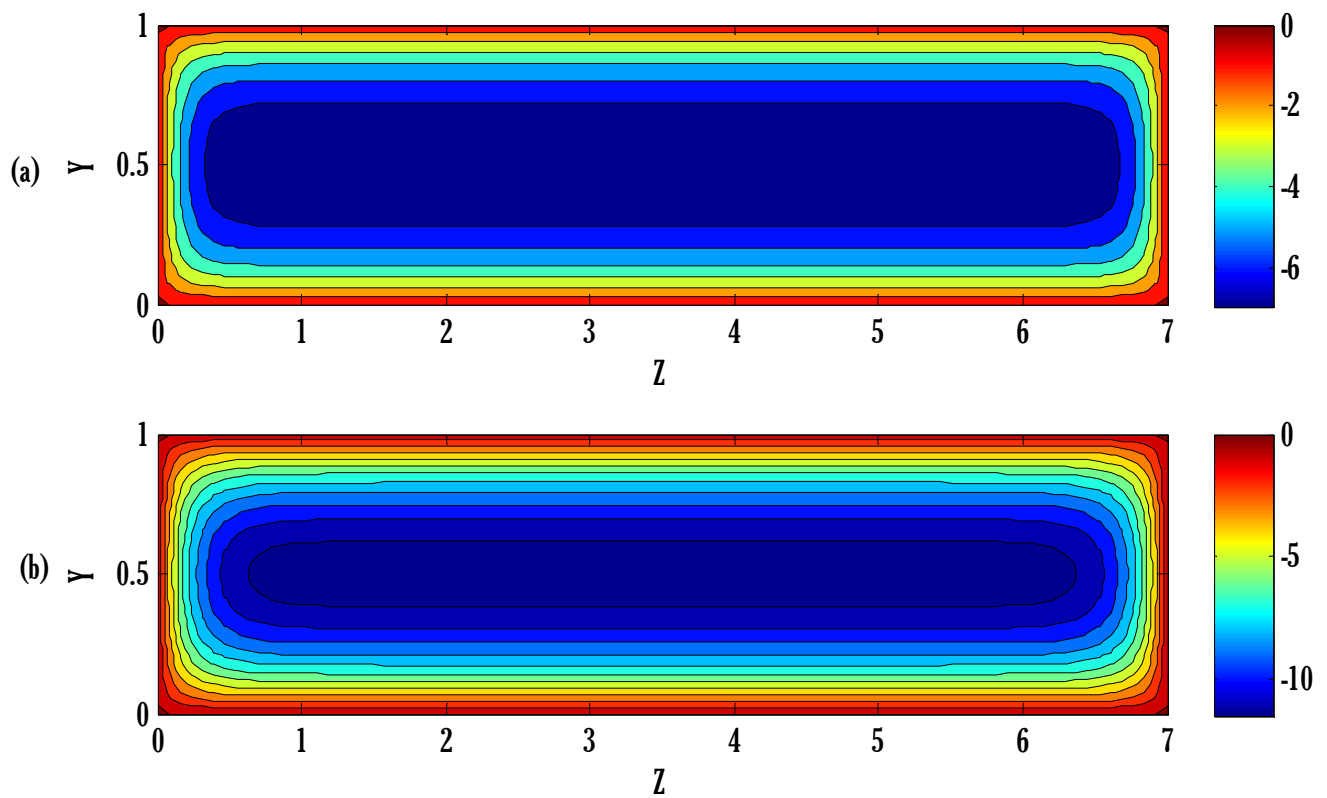


Figure 3. Velocity of the flow at different times (a) $\tau = 0.4998$, (b) $\tau = 1$ using $N_\tau = 2500$, $N_Y = 40$, $N_Z = 900$, $\partial P / \partial X = -15$.

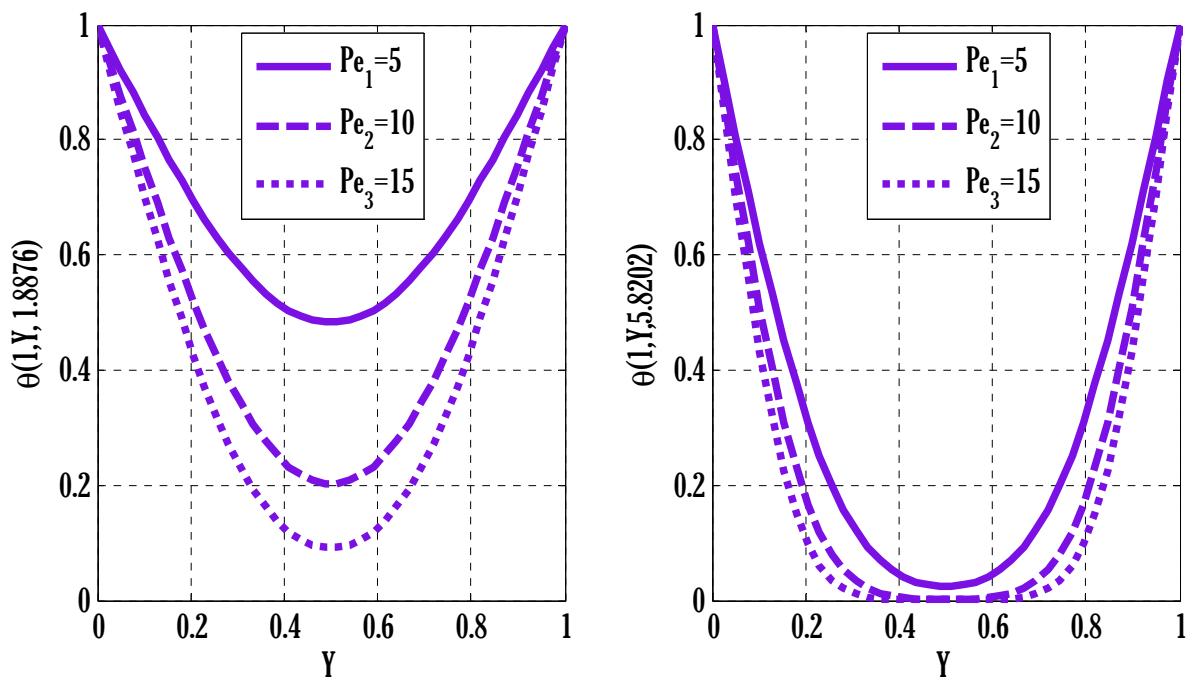


Figure 4. Impact of thermal Péclet number on the temperature of the flow using $N_\tau = 3500$, $N_Y = 40$, $N_Z = 900$.

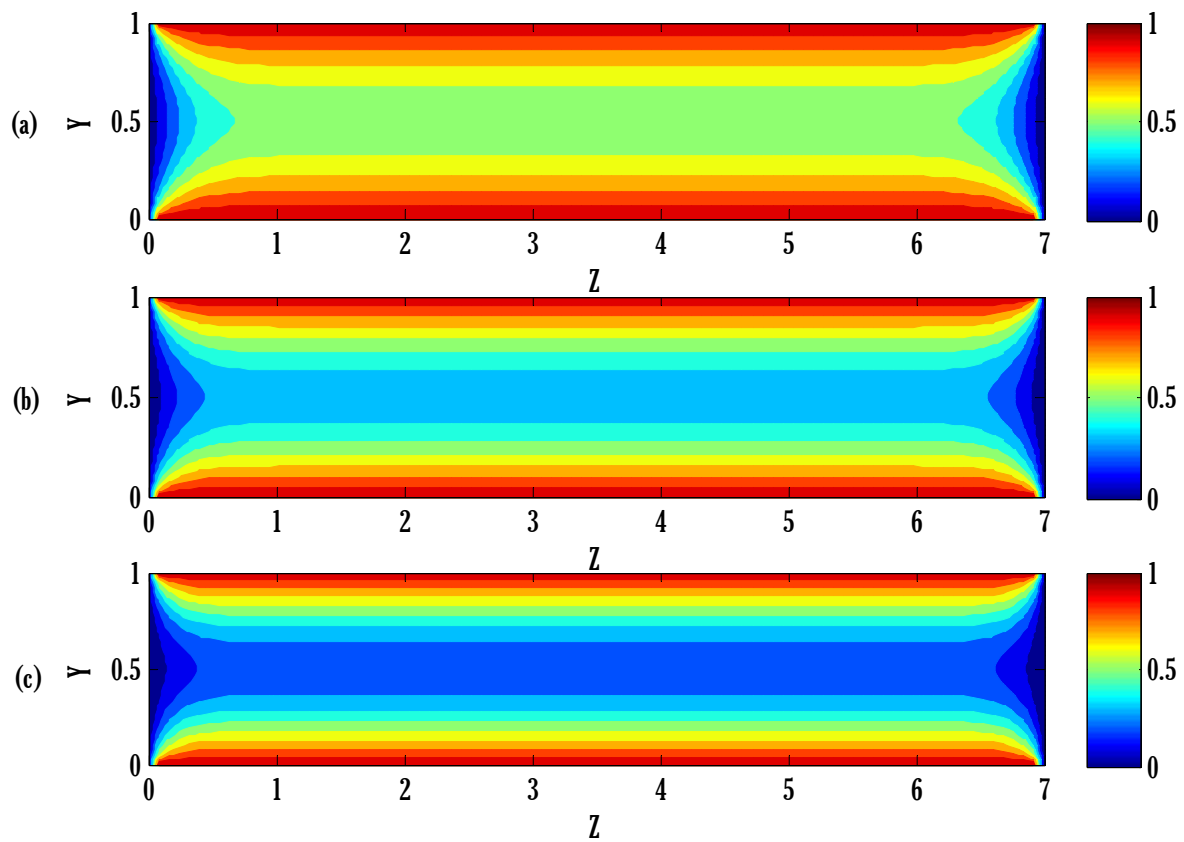


Figure 5. Impact of thermal Péclet number on contours of flow's temperature at (a) $Pe_1 = 10$, (b) $Pe_1 = 15$, (c) $Pe_1 = 20$ using $N_\tau = 3500$, $N_Y = 40$, $N_Z = 900$, $t_f = 1$.

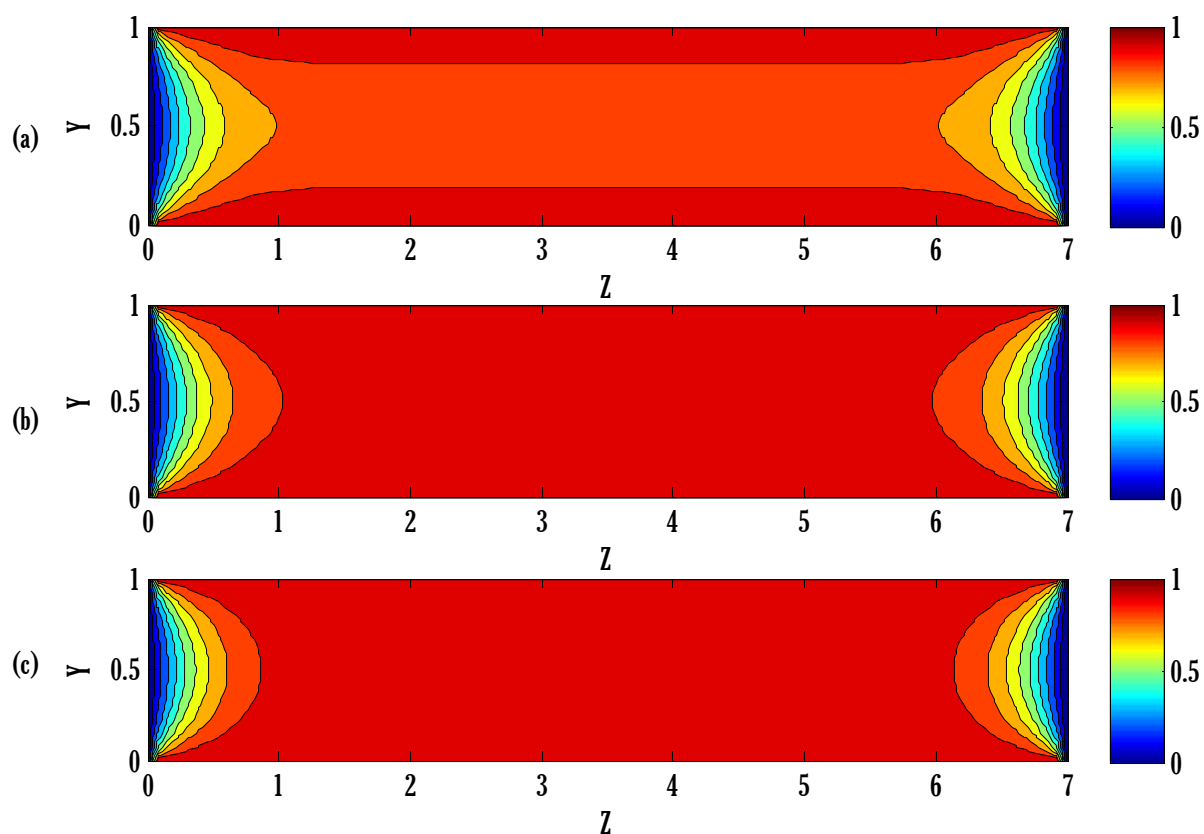


Figure 6. Contours of flow's temperature at different times (a) $\tau = 0.9999$, (b) $\tau = 1.4999$, (c) $\tau = 2$ using $N_\tau = 8000$, $N_Y = 40$, $N_Z = 900$, $Pe_1 = 5$.

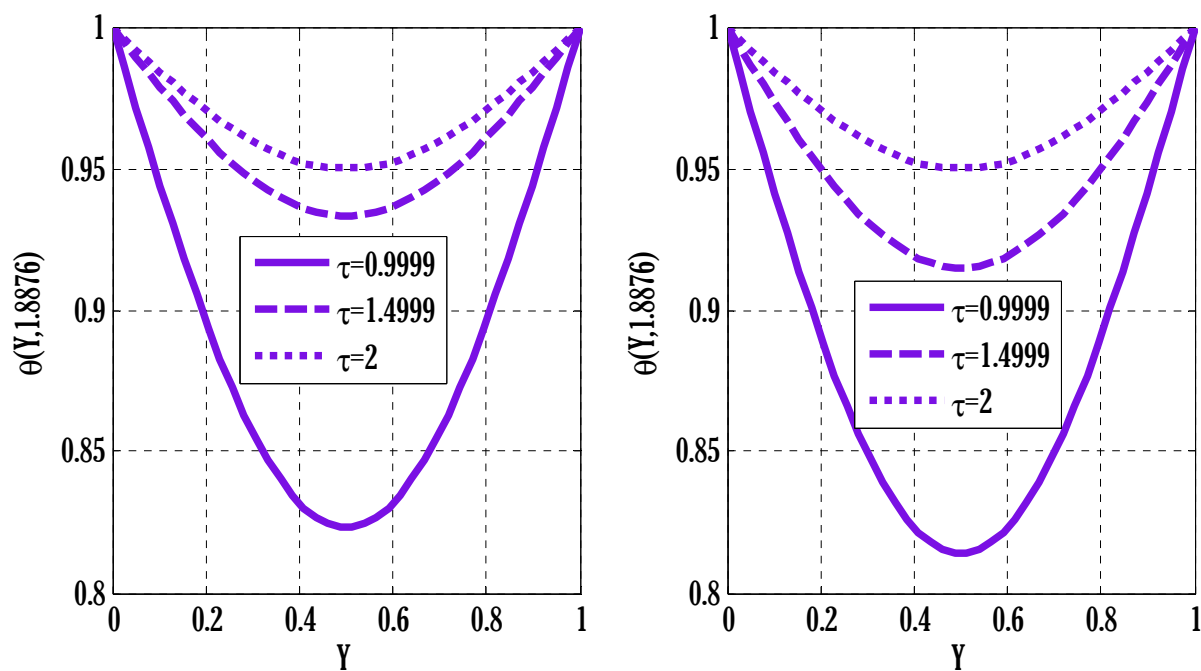


Figure 7. Flow temperature at different times using $N_\tau = 8000$, $N_Y = 40$, $N_Z = 900$, $Pe_1 = 5$.

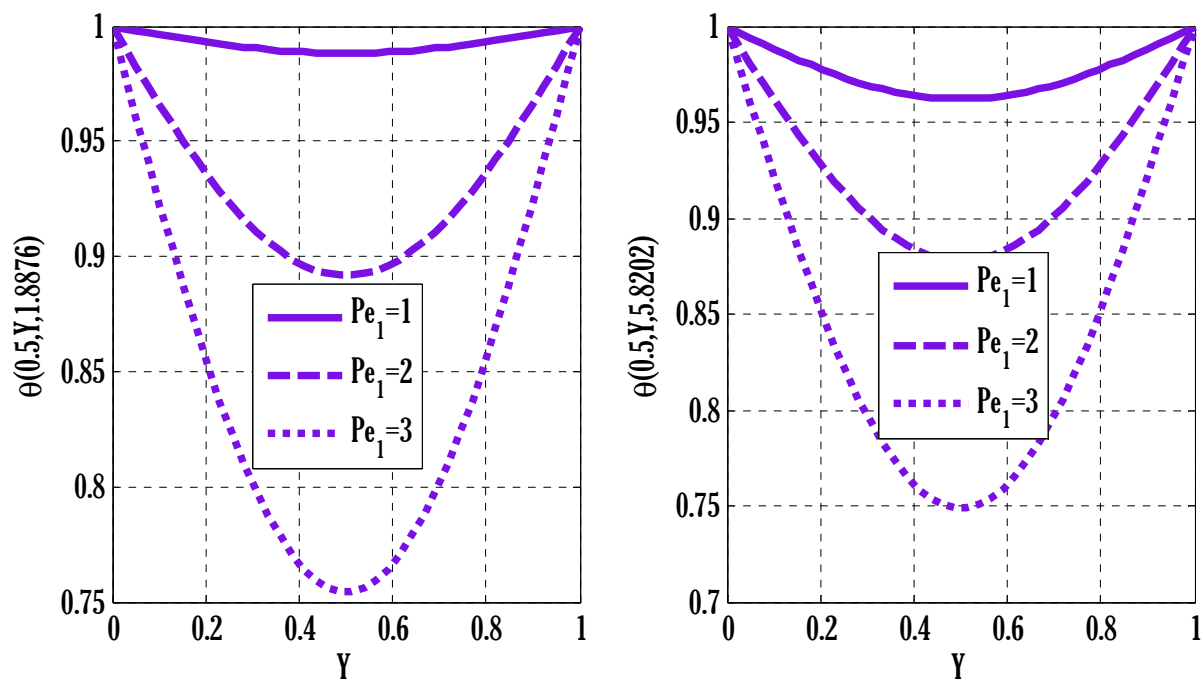


Figure 8. Impact of thermal Péclet number on flow temperature using $N_\tau = 10000$, $N_Y = 40$, $N_Z = 900$, $Pe_1 = 5$.

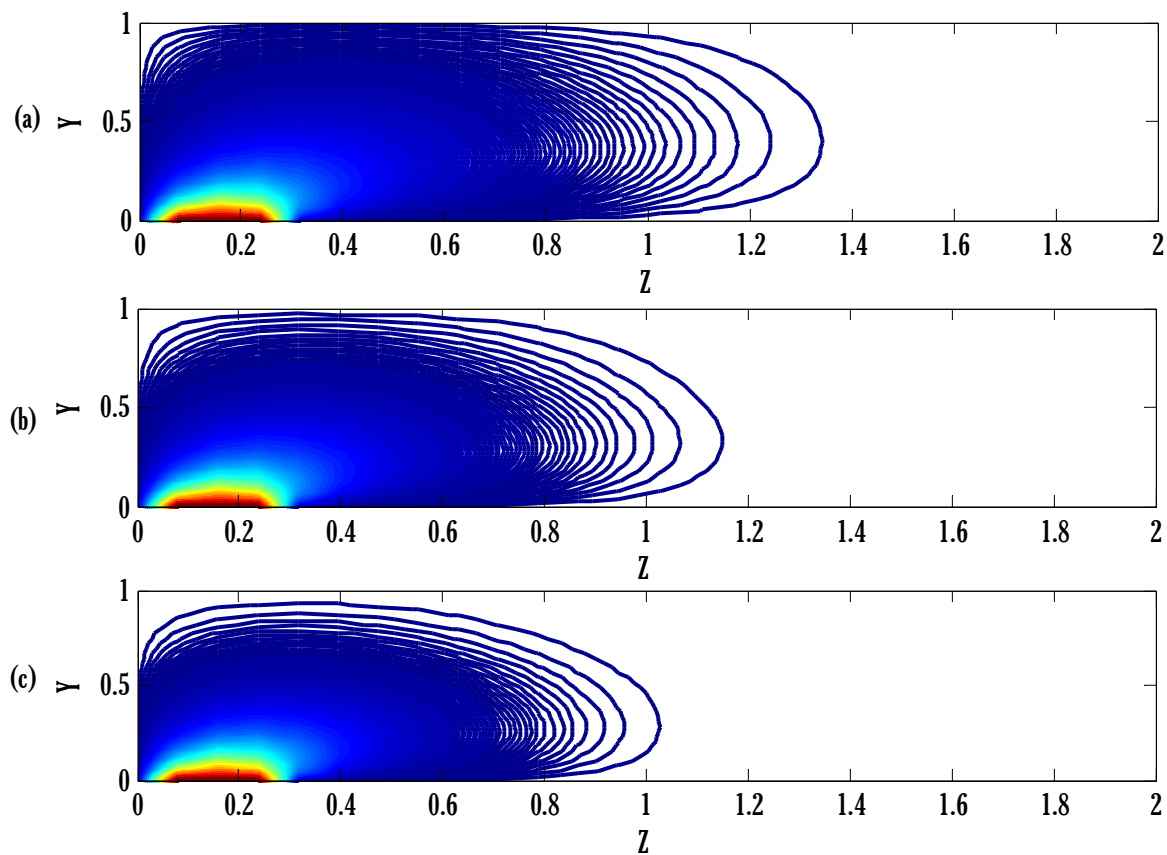


Figure 9. Impact of solutal Péclet number on contours of concentration at (a) $Pe_2 = 10$, (b) $Pe_2 = 15$, (c) $Pe_2 = 20$ using $N_\tau = 3000$, $N_Y = 40$, $N_Z = 900$, $\gamma = 4$, $t_f = 1$.

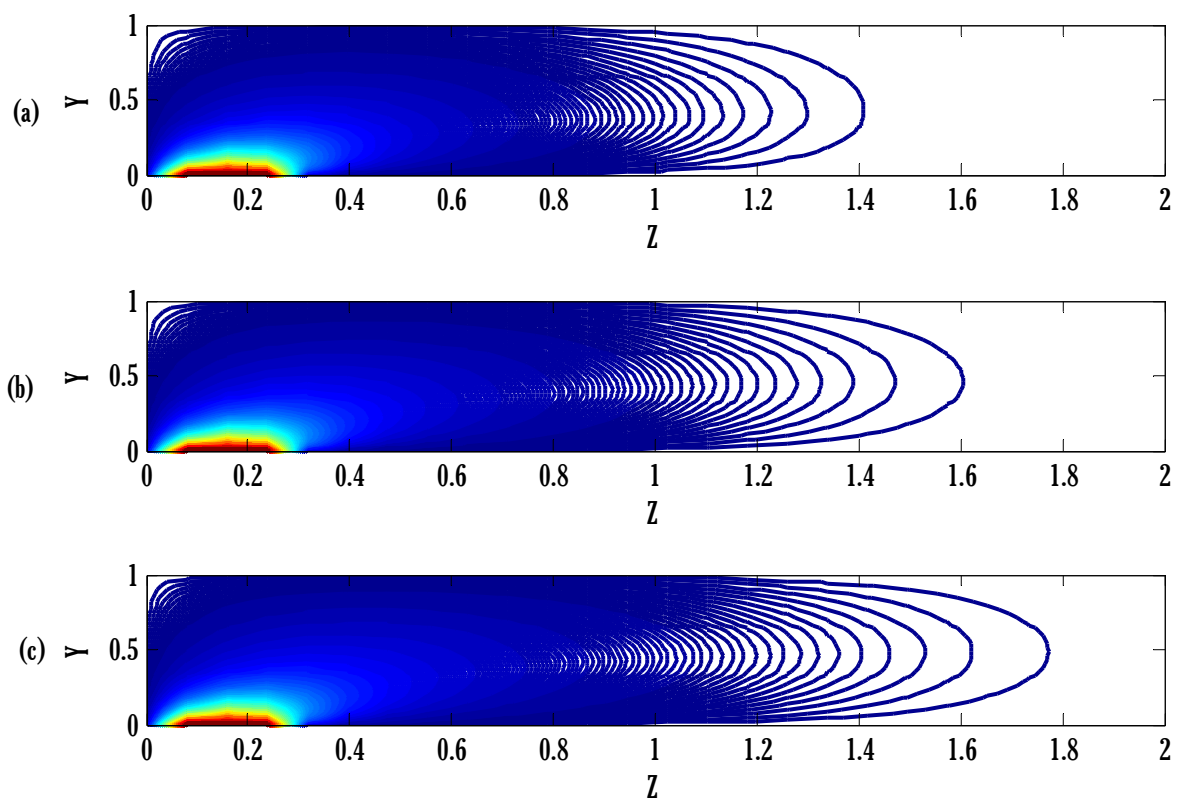


Figure 10. Concentration contours at different times at (a) $\tau = 0.5999$, (b) $\tau = 0.8$, (c) $\tau = 1$ using $N_\tau = 5000$, $N_Y = 40$, $N_Z = 900$, $\gamma = 4$, $t_f = 1$, $Pe_2 = 5$.

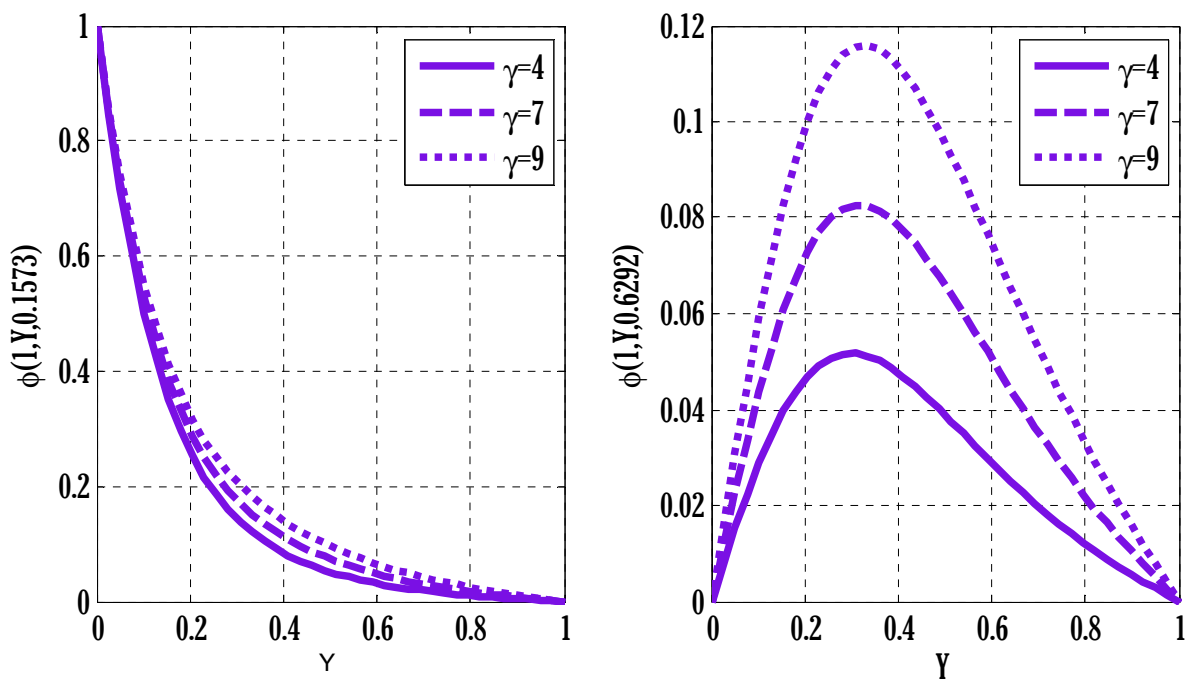


Figure 11. Impact of reaction rate parameter on concentration using $N_\tau = 3000$, $N_Y = 40$, $N_Z = 900$, $\gamma = 4$, $Pe_2 = 10$.

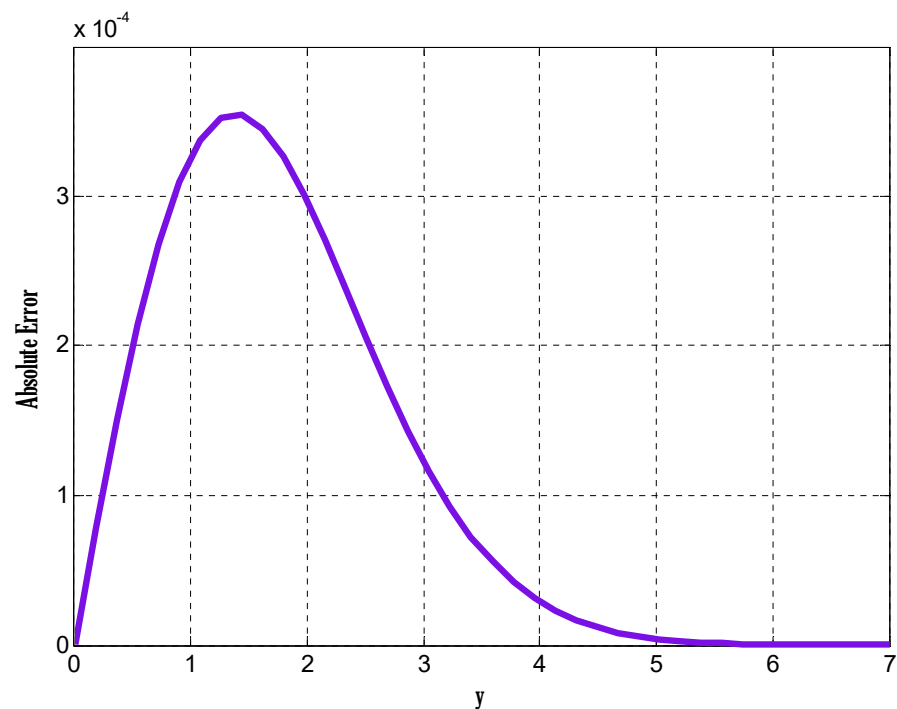


Figure 12. Absolute error obtained by the proposed scheme using $a = \frac{1}{2}$, $N_t = 350$, $N_y = 40$, $t_f = 1$.

Due to transferring of heat, the temperature approaches its maximum values at both locations of chosen z coordinate by time. Effect of thermal Péclet number on the temperature of the flow is shown in Figure 8.

These two-dimensional graphs show that temperature is decreasing by growing values of thermal Péclet number. The effect of solutal Péclet number on concentration is shown in Figure 9.

The mass transfer is better at smaller values of the solutal Péclet number. This is the consequence of decreasing mass diffusivity by increasing solutal Péclet number because both are inversely proportional to each other. Figure 10 shows the contours of concentration with time. The concentration is maximum at the specified location at z -axis due to imposed boundary conditions. The transfer of mass from this location to the adjacent layers of fluid flow can be seen in Figure 10.

The effect of the reaction rate parameter on concentration can be seen in Figure 11. The dual behavior of concentration can be seen in Figure 11.

For verification of the code for the proposed scheme for a time-dependent partial differential equation, the following example is considered:

$$\frac{\partial v}{\partial t} = \frac{\partial^2 v}{\partial y^2} \quad (83)$$

subject to the boundary conditions

$$v(t, 0) = 1 \quad \text{and} \quad v \rightarrow 0 \text{ when } y \rightarrow \infty \quad (84)$$

and using zero as the initial condition. The problem is solved using the proposed scheme in time and fourth-order spatial discretization except at those grid points where fourth-order central spatial discretization cannot be employed. The exact solution of the problem (83) and (84) is available. The comparison of the proposed scheme with the exact solution is given in Figure 12.

Figure 12 shows the absolute error produced by the proposed scheme, which is obtained by finding the absolute value for the difference between numerical and exact solutions. Figure 13 demonstrates the usefulness of the proposed scheme (4), which is the combination of the existing second-order scheme (2) and a modification given in the existing DuFort method (3). The proposed scheme produces a better stability region, which is evidence of the proposed strategy in Figure 13. The existing second-order scheme does not converge on chosen temporal step size. However, the proposed scheme (4) converges on the same temporal step size, but the temporal order of the proposed scheme (4) is reduced to one due to first-order modification (3). In the caption of Figure 13, N_t , N_y , and t_f denote the number of time levels, grid points, and final time, respectively.

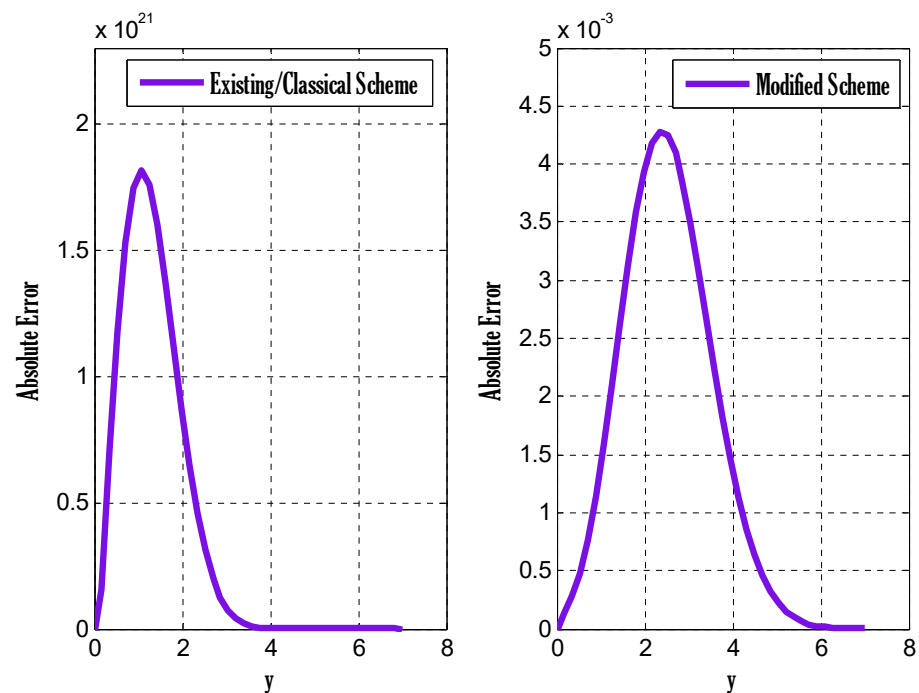


Figure 13. Comparison of existing/classical Adams–Bashforth scheme and proposed scheme using $N_t = 50$, $N_y = 40$, $t_f = 1$.

8. Conclusions

An explicit class of second to fifth-order accurate in-time schemes was proposed for time-dependent PDEs. The stability of the second-order in time and space scheme for the parabolic linear PDE was found. Additionally, a modification was suggested so that the modified proposed scheme permits a little larger stability region for time-dependent PDEs. Moreover, stability conditions of the linearized non-dimensional form of the present model were found, and the convergence condition of the present scheme for the considered system of PDEs in the flow phenomenon was found. Some related discussions drew plots of velocity, temperature, and concentration contours, along with temperature and concentration profiles. In addition, the proposed method was easy to implement and can be used in a larger class of partial differential equations seen in both practical and theoretical contexts.

Author Contributions: Conceptualization—Y.N.; funding acquisition—W.S.; investigation, software, writing (review and editing), methodology, and writing (original draft)—Y.N.; methodology—M.S.A.; project administration—W.S.; resources—W.S.; supervision—M.S.A.; visualization—W.S.; writing (review and editing)—M.B. All authors have read and agreed to the published version of the manuscript.

Funding: This work was supported by a Seed Project research grant from Prince Sultan University, Saudi Arabia (SEED-2022-CHS-100).

Institutional Review Board Statement: Not applicable.

Informed Consent Statement: Not applicable.

Data Availability Statement: The manuscript includes all relevant data and implementation information.

Acknowledgments: The authors express their gratitude to Prince Sultan University for facilitating the publication of this article through the Theoretical and Applied Sciences Lab.

Conflicts of Interest: The authors declare no conflict of interest.

References

- Malapati, V.; Polarapu, P. Unsteady MHD free convective heat and mass transfer in a boundary layer flow past a vertical permeable plate with thermal radiation and chemical reaction. *Procedia Eng.* **2015**, *127*, 191–199. [\[CrossRef\]](#)
- Davidson, P.A. *An Introduction to Magnetohydrodynamics*; Cambridge University Press: New York, NY, USA, 2001.
- Dogonchi, A.S.; Ganji, D.D. Impact of Cattaneo—Christov heat flux on MHD nanofluid flow and heat transfer between parallel plates considering thermal radiation effect. *J. Taiwan Inst. Chem. Eng.* **2017**, *52*, 52–64. [\[CrossRef\]](#)
- Dogonchi, A.S.; Divsalar, K.; Ganji, D.D. Flow and heat transfer of MHD nanofluid between parallel plates in the presence of thermal radiation. *Comput. Methods Appl. Mech. Eng.* **2016**, *310*, 58–76. [\[CrossRef\]](#)
- Ghasemi, K.; Siavashi, M. MHD nanofluid free convection and entropy generation in porous enclosures with different conductivity ratios. *J. Magn. Magn. Mater.* **2017**, *442*, 474–490. [\[CrossRef\]](#)
- Sarma, R.; Gaikwad, H.; Mondal, P.K. Effect of conjugate heat transfer on entropy generation in slip-driven microflow of power law fluids. *Nanoscale Microscale Thermophys. Eng.* **2017**, *21*, 26–44. [\[CrossRef\]](#)
- Reddy, P.B.A.; Suneetha, S.; Reddy, N.B. Numerical study of magnetohydrodynamics (MHD) boundary layer slip flow of a Maxwell nanofluid over an exponentially stretching surface with convective boundary condition. *Propuls. Power Res.* **2017**, *6*, 259–268. [\[CrossRef\]](#)
- Hussain, A.; Malik, M.Y.; Salahuddin, T.; Rubab, A.; Khan, M. Effects of viscous dissipation on MHD tangent hyperbolic fluid over a non-linear stretching sheet with convective boundary conditions. *Results Phys.* **2017**, *7*, 3502–3509. [\[CrossRef\]](#)
- Khan, M.; Malik, M.Y.; Salahuddin, T.; Hussain, A. Heat and mass transfer of Williamson nanofluid flow yield by an inclined Lorentz force over a non-linear stretching sheet. *Results Phys.* **2018**, *8*, 862–868. [\[CrossRef\]](#)
- Soid, S.K.; Ishak, A.; Pop, I. MHD flow and heat transfer over a radially stretching/shrinking disk. *Chin. J. Phys.* **2016**, *56*, 58–66. [\[CrossRef\]](#)
- Narayana, P.V.S.; Venkateswarlu, B.; Devika, B. Chemical reaction and heat source effects on MHD oscillatory flow in an irregular channel. *Ain Shams Eng. J.* **2016**, *7*, 1079–1088.
- Nayak, M.K.; Akbar, N.S.; Tripathi, D.; Khan, Z.H.; Pandey, V.S. MHD 3D free convective flow of nanofluid over an exponentially stretching sheet with chemical reaction. *Adv. Powder Technol.* **2017**, *9*, 2159–2166. [\[CrossRef\]](#)
- Yu, H.; Son, G.; Shim, W. Numerical simulation of droplet merging and chemical reaction in a porous medium. *Int. Commun. Heat Mass Transf.* **2017**, *89*, 154–164. [\[CrossRef\]](#)
- Hayat, T.; Waqas, M.; Khan, M.I.; Alsaedi, A. Impacts of constructive and destructive chemical reactions in magnetohydrodynamic (MHD) flow of Jeffrey liquid due to non-linear radially stretched surface. *J. Mol. Liq.* **2017**, *225*, 302–310. [\[CrossRef\]](#)
- Wen, X.; Wang, H.; Luo, Y.; Luo, K.; Fan, J. Numerical investigation of the effects of volatile matter composition and chemical reaction mechanism on pulverized coal combustion characteristics. *Fuel* **2017**, *210*, 695–704. [\[CrossRef\]](#)
- Tlili, I.; Khan, W.A.; Khan, I. Multiple slips effects on MHD SA-Al₂O₃ and SA-Cu non-Newtonian nanofluids flow over a stretching cylinder in porous medium with radiation and chemical reaction. *Results Phys.* **2018**, *8*, 213–222. [\[CrossRef\]](#)
- Sambath, P.; Pullepu, B.; Hussain, T.; Shehzad, S.A. Radiated chemical reaction impacts on natural convective MHD mass transfer flow induced by a vertical con. *Results Phys.* **2018**, *8*, 304–315. [\[CrossRef\]](#)
- Kerboua, K.; Hamdaoui, O. Influence of reactions heats on variation of radius, temperature, pressure and chemical species amounts within a single acoustic cavitation bubble. *Ultrason. Sonochem.* **2018**, *41*, 447–457. [\[CrossRef\]](#)
- Khan, M.; Shahid, A.; Malik, M.Y.; Salahuddin, T. Chemical reaction for Carreau-Yasuda nanofluid flow past a non-linear stretching sheet considering Joule heating. *Results Phys.* **2018**, *8*, 1124–1130. [\[CrossRef\]](#)
- Acharya, N.; Das, K.; Kundu, P.K. Cattaneo—Christov intensity of magnetised upperconvected Maxwell nanofluid flow over an inclined stretching sheet: A generalised Fourier and Fick’s perspective. *Int. J. Mech. Sci.* **2017**, *230*, 167–173. [\[CrossRef\]](#)
- Khan, M.; Shahid, A.; Malik, M.Y.; Salahuddin, T. Thermal and concentration diffusion in Jeffery nanofluid flow over an inclined stretching sheet: A generalized Fourier’s and Fick’s perspective. *J. Mol. Liq.* **2018**, *251*, 7–14. [\[CrossRef\]](#)
- Ellahi, R.; Bhatti, M.M.; Vafai, K. Effects of heat and mass transfer on peristaltic flow in a non-uniform rectangular duct. *Int. J. Heat Mass Transf.* **2014**, *71*, 706–719. [\[CrossRef\]](#)
- Hina, S.; Mustafa, M.; Hayat, T.; Alsaedi, A. Peristaltic transport of Powell-Eyring fluid in a curved channel with heat/mass transfer and wall properties. *Int. J. Heat Mass Transf.* **2016**, *101*, 156–165. [\[CrossRef\]](#)
- Nadeem, S.; Akbar, N.S.; Bibi, N.; Ashiq, S. Influence of heat and mass transfer on peristaltic flow of a third order fluid in a diverging tube. *Commun. Nonlinear Sci. Numer. Simul.* **2010**, *15*, 2916–2931. [\[CrossRef\]](#)
- Hoffmann, K.A.; Chiang, S.T. *Computational Fluid Dynamics (Vol. 1)*; Engineering Education System: Wichita, KS, USA, 2000.
- Sarma, R.; Mondal, P.K. Entropy generation minimization in a pressure-driven microflow of viscoelastic fluid with slippage at the wall: Effect of conjugate heat transfer. *J. Heat Transf.* **2018**, *140*, 052402. [\[CrossRef\]](#)
- Sarma, R.; Nath, A.J.; Konwar, T.; Mondal, P.K.; Wongwises, S. Thermo-hydrodynamics of a viscoelastic fluid under asymmetrical heating. *Int. J. Heat Mass Transf.* **2018**, *125*, 515–524. [\[CrossRef\]](#)
- Nayak, M.K. MHD 3D flow and heat transfer analysis of nanofluid by shrinking surface inspired by thermal radiation and viscous dissipation. *Int. J. Mech. Sci.* **2017**, *124*, 185–193. [\[CrossRef\]](#)
- Zangoee, M.R.; Hosseinzadeh, K.; Ganji, D.D. Hydrothermal analysis of MHD nanofluid (TiO₂-GO) flow between two radiative stretchable rotating disks using AGM. *Case Stud. Therm. Eng.* **2017**, *56*, 621–627. [\[CrossRef\]](#)

-
30. Nawaz, Y. Development of new and modified numerical methods for hyperbolic conservation laws. *Numer. Heat Transf. Part B Fundam.* **2019**, *76*, 224–251. [[CrossRef](#)]
 31. Nawaz, Y.; Arif, M.S.; Shatanawi, W.; Nazeer, A. An explicit fourth-order compact numerical scheme for heat transfer of boundary layer flow. *Energies* **2021**, *14*, 3396. [[CrossRef](#)]
 32. Nawaz, Y.; Arif, M.S.; Shatanawi, W.; Ashraf, M.U. A Fourth Order Numerical Scheme for Unsteady Mixed Convection Boundary Layer Flow: A Comparative Computational Study. *Energies* **2022**, *15*, 910. [[CrossRef](#)]